Mon. Not. R. Astron. Soc. **397,** 1836–1851 (2009) doi:10.1111/j.1365-2966.2009.15123.x

The ultraluminous state

Jeanette C. Gladstone,★ Timothy P. Roberts and Chris Done

Department of Physics, University of Durham, South Road, Durham DH1 3LE

Accepted 2009 May 21. Received 2009 May 21; in original form 2009 March 27

ABSTRACT

We revisit the question of the nature of ultraluminous X-ray sources (ULXs) through a detailed investigation of their spectral shape, using the highest quality X-ray data available in the *XMM–Newton* public archives ($\gtrsim$10 000 counts in their EPIC spectrum). We confirm that simple spectral models commonly used for the analysis and interpretation of ULXs (power-law continuum and multicolour disc blackbody models) are inadequate in the face of such high-quality data. Instead we find two near ubiquitous features in the spectrum: a soft excess and a rollover in the spectrum at energies above 3 keV. We investigate a range of more physical models to describe these data. Slim discs which include radiation trapping (approximated by a *p*-free disc model) do not adequately fit the data, and several objects give unphysically high disc temperatures ($kT_{\rm in} > 3$ keV). Instead, disc plus Comptonized corona models fit the data well, but the derived corona is cool and optically thick ($\tau \sim 5$–30). This is unlike the $\tau \sim 1$ coronae seen in Galactic binaries, ruling out models where ULXs are powered by sub-Eddington accretion on to an intermediate-mass black hole despite many objects having apparently cool disc temperatures. We argue that these observed disc temperatures are not a good indicator of the black hole mass as the powerful, optically thick corona drains energy from the inner disc and obscures it. We estimate the intrinsic (corona-less) disc temperature, and demonstrate that in most cases it lies in the regime of stellar mass black holes. These objects have spectra which range from those similar to the highest mass accretion rate states in Galactic binaries (a single peak at 2–3 keV) to those which clearly have two peaks, one at energies below 1 keV (from the outer, un-Comptonized disc) and one above 3 keV (from the Comptonized, inner disc). However, a few ULXs have a significantly cooler corrected disc temperature; we suggest that these are the most extreme stellar mass black hole accretors, in which a massive wind completely envelopes the inner-disc regions, creating a cool photosphere. We conclude that ULXs provide us with an observational template for the transition between Eddington and super-Eddington accretion flows, with the latter occupying a new *ultraluminous* accretion state.

Key words: accretion, accretion discs – black hole physics – X-rays: binaries – X-rays: galaxies.

1 INTRODUCTION

Ultraluminous X-ray sources (ULXs) are bright X-ray sources with $L_{\rm X} > 10^{39}$ erg s^{-1}. These objects are not associated with the nuclei of galaxies, so are not powered by accretion on to a central supermassive black hole, but are too bright for sub-Eddington accretion on to stellar mass black holes that radiate isotropically. An obvious solution is therefore an object intermediate in mass between that of stellar mass and supermassive black holes: intermediate-mass black holes (IMBHs), of mass $\sim 10^2$–10^4 M$_\odot$, accreting at sub-Eddington rates (e.g. Colbert & Mushotzky 1999; Miller & Colbert 2004). Various pathways for the formation of IMBHs have been suggested, both primordial (from the collapse of Population III stars; Madau & Rees 2001) and ongoing (runaway mergers of massive stars and their subsequent collapse to a massive black hole, in the densest star-formation regions, e.g. Portegies-Zwart, Dewi & Maccarone 2004), but problems persist in producing sufficient numbers of IMBHs to tally with those seen in the local Universe (Madhusudhan et al. 2006). Thus, an alternative must be considered that the majority of ULXs are single stellar remnant black holes that accrete material from a close companion star, probably at super-Eddington rates and/or with their X-ray emission subject to some degree of geometric beaming (e.g. King et al. 2001; Begelman 2002; see also Roberts 2007 and references therein). More extreme beaming from relativistic jets seems unlikely due to the number of

★E-mail: j.c.gladstone@durham.ac.uk

unbeamed sources that would need to be present in systems such as the Cartwheel galaxy (King 2004).

Either conclusion remains controversial or the question of what underlies ULXs can only be ultimately solved by a direct mass measurement based on constraints placed by the binary orbit. Until this is achieved, more indirect methods of determining the mass must be used in an attempt to constrain the nature of these accreting systems. A common method is to use the temperature of the accretion disc emission, together with its luminosity, to determine the mass as Shakura–Sunyaev models predict the disc temperature $kT \sim (M/10\,\mathrm{M}_\odot)^{-1/4}\,(L/L_{\mathrm{Edd}})^{1/4}$ keV (Shakura & Sunyaev 1973). The highest signal-to-noise ratio spectra of ULXs can often be well fitted by composite models of a disc together with a hard ($\Gamma < 2$) tail, with the low measured disc temperature of $\sim$0.2 keV implying a high black hole mass of $\sim 10^3$ $\mathrm{M}_\odot$ (e.g. Kaaret et al. 2003; Miller et al. 2003, 2004). This supports the IMBH interpretation, and the resulting very sub-Eddington accretion rates ($<0.1L_{\mathrm{Edd}}$) would most likely be associated with the low/hard state in black hole binaries (BHBs), consistent with the observed hard tail.

However, it is also clear from many studies of BHBs that disc models only give reliable results when the X-ray spectrum is dominated by this component (the high/soft or thermal-dominant state) (Done & Kubota 2006). The derived disc temperature is increasingly distorted as the tail increases in importance, with very low temperature, high-luminosity discs (implying a much larger mass black hole than is known to be present!) seen when both tail and disc are strongest, as in the very high or steep power-law state (Kubota & Done 2004; Done & Kubota 2006). The ULX spectral decompositions of Miller et al. (2004) all have strong tails ($\gtrsim$80 per cent of the 0.3–10 keV flux; Stobbart, Roberts & Wilms 2006, hereafter SRW06), so a straightforward interpretation of the derived disc parameters is unlikely to give a robust mass estimator.[1]

However, the best data also show the limitations of this simple spectral fitting. There is clear evidence for curvature of the tail at the highest energies, with a deficit of photons above 5 keV (Roberts et al. 2005; SRW06; Miyawaki et al. 2009). Such curvature is never seen in the low/hard state at these low energies. Only the very high state shows curvature at such low energies, but these generally have spectra which are steep. The temporal variability also does not correspond to that expected from an IMBH in this (or any other) state. The simple disc and tail spectral decomposition shows that the tail dominates the *XMM–Newton* band pass, so by analogy with the BHBs this emission should be strongly variable. Yet many *XMM–Newton* ULX light curves show only upper limits on the variability power consistent with the Poisson noise level for the data (Feng & Kaaret 2005). Thus, neither the spectral nor variability properties convincingly correspond to any of the accretion states known in BHBs, making it unlikely that ULXs are powered by sub-Eddington flows on to an IMBH (Roberts 2007).

This conclusion is strongly supported by population studies of ULXs. The sheer numbers observed in starburst galaxies together with their short lifetimes (implied by their location in regions of active star formation) mean that an unrealistically large underlying population of IMBHs must be present (King 2004). Instead it is much more likely that the bulk of the population is the most extreme examples of high-mass X-ray binaries (HMXBs) which somehow exceed the Eddington limit. The high-mass companion gives a natural origin for the high-mass transfer rates required to power the observed luminosities (Rappaport, Podsiadlowski & Pfahl 2005). It also explains the association of ULXs with star-forming regions (Fabbiano, Zezas & Murray 2001; Lira et al. 2002; Gao et al. 2003) and the unbroken luminosity function connecting ULXs to the standard X-ray binary population (Grimm, Gilfanov & Sunyaev 2003). Indeed, direct evidence for ULXs possessing high-mass donor stars comes from the identification of luminous, blue optical stellar counterparts to several nearby ULXs (e.g. Liu, Bregman & Seitzer 2004; Kuntz et al. 2005; Roberts, Levan & Goad 2008).

Many ULX host galaxies have subsolar abundances (e.g. Lee et al. 2006). The lower opacity of subsolar material means that massive stars lose less mass through winds during their evolution, so potentially can collapse to form a relatively high-mass black hole at the end of their stellar lifetime, with $M_{\mathrm{BH}} \lesssim 80\,\mathrm{M}_\odot$ (Fryer & Kalogera 2001; Heger et al. 2003; Belczynski, Sadowski & Rasio 2004; Belczynski et al. 2009). One such large stellar mass black hole was discovered in IC 10 X-1, a Wolf–Rayet BHB. A radial velocity curve was constructed from repeated optical observations, which provided a mass estimate of 23–34 $\mathrm{M}_\odot$ (Prestwich et al. 2007; Silverman & Filippenko 2008). None the less, even such massive stellar remnant black holes are required to be accreting at super-Eddington rates to explain the observed luminosities of the brightest ULXs. Thus, the accretion flows in ULXs may not simply be scaled-up versions of those seen in BHBs, as would be the case for the IMBH[2] model where the flows are sub-Eddington. Instead, observation of ULXs may allow us to probe a new regime of accretion physics, a new 'ultraluminous state' (Roberts 2007; Soria 2007).

Here we revisit the question of what the X-ray spectra of ULXs can tell us about the nature of their accretion flows, and how this constrains the nature of the accreting object, by utilizing the best data currently available in the *XMM–Newton* public archives. We choose to use the best available data as previous studies of samples of ULXs (e.g. Berghea et al. 2008), whilst providing interesting results, are ultimately limited in the conclusions they can draw by the moderate signal-to-noise ratio of many ULX spectra. By using only the highest quality data from the widest band pass, highest sensitivity instruments available we can hope to avoid the ambiguity of previous analyses, and make definitive statements on the accretion processes in ULXs. This paper is arranged as follows. First, we outline the sample selection and the data reduction processes (Sections 2 and 3). Next, we investigate the X-ray spectra using a variety of empirical and physical models, in order to both clarify the morphology of ULX spectra in the putative ultraluminous state and investigate the physical processes underlying this phenomenon (Section 4). Finally, we discuss the implications of our results for the nature of ULXs (Section 5).

[1] It should also be noted that band pass is a potential problem in comparing ULX results with those of BHBs. Given their high fluxes, Galactic sources have been most commonly studied in detail using telescopes such as *RXTE*, so are generally characterized by their behaviour in the 3–20 keV regime. The more distant (and hence fainter) ULXs instead require the more sensitive, high-spatial-resolution telescopes of *Chandra* and *XMM–Newton* for detailed studies, whose CCD detectors cover the 0.3–10 keV band. This difference in typical energy range between the ULX and BHB data means that any comparison between the two must be made with care.

[2] Here and throughout the paper, we distinguish IMBHs as BHs with masses $>100\,\mathrm{M}_\odot$, as suggested by the X-ray spectral modelling of Miller et al. (2003) and subsequent work. Such black holes are not formed at the endpoint of a recent single stellar evolution, but require more exotic origins such as stellar mergers in a young super-star cluster (e.g. Portegies-Zwart & McMillan 2002) or formation from primordial Population III stars in the high-redshift Universe (Madau & Rees 2001).

Table 1. The ULX sample.

Source	Alternative names	RA (J2000)	Dec. (J2000)	$N_{\rm H}{}^a$ (10^{20} cm^{-2})	d^b (Mpc)	$L_{\rm X}{}^c$ (10^{39} erg s^{-1})
NGC 55 ULX[1]	XMMU J001528.9−391319[2] NGC 55 6[3] Source 7[4]	00 15 28.9	−39 13 19.1	1.71	1.78(i)	1.1
M33 X-8[1]	CXOU J013351.0+303937[5] NGC 598 ULX1[6] Source 3[7]	01 33 50.8	+30 39 37.1	5.58	0.70(i)	1.0
NGC 1313 X-1[1]	IXO 7[8] Source 4[7]	03 18 20.0	−66 29 11.0	3.90	3.70(i)	3.7
NGC 1313 X-2[1]	IXO 8[8] NGC 1313 ULX3[9] Source 5[7]	03 18 22.3	−66 36 03.8	3.90	3.70(i)	4.7
IC 342 X-1[10]	CXOU J034555.7+680455[11] IXO 22[8] PGC 13826 ULX3[9]	03 45 55.5	+68 04 54.2	31.1	3.3(ii)	2.8
NGC 2403 X-1[1]	CXOU J073625.5+653540[12] Source 21[13] NGC 2403 X2[9]	07 36 25.6	+65 35 40.0	4.17	4.20(i)	2.4
Ho II X-1[1]	IXO 31[8] PGC 23324 ULX1[9] CXOU J081928.99+704219.4[12]	08 19 29.0	+70 42 19.3	3.42	4.50(i)	14.4
M81 X-6[1]	NGC 3031 ULX1[6] CXOU J095532.98+690033.4[12]	09 55 32.9	+69 00 33.3	4.16	3.63(iii)	2.2
Ho IX X-1[1]	M81 X-9[1] NGC 3031 10[14] IXO 34[8] H 44[15] Source 17[7]	09 57 53.2	+69 03 48.3	4.06	3.55(i)	7.5
NGC 4559 X-1[1]	IXO 65[8] CXOU J123551.71+275604.1[12] X-7[16]	12 35 51.7	+27 56 04.1	1.49	9.70(i)	8.0
NGC 5204 X-1[1]	IXO 77[8] CXOU J132938.61+582505.6[12] Source 23[7]	13 29 38.6	+58 25 05.7	1.39	4.80(i)	5.3
NGC 5408 X-1[17]	J140319.606−412259.572[17] Source 25[7]	14 03 19.6	−41 22 59.6	5.67	4.80(iv)	3.7

Note. [a]Absorption column values taken from Dickey & Lockman (1990) using WEBPIMMS. [b]Figures shown in brackets relate to the following references, from which the assumed distance was taken: (i) SRW06, (ii) Saha, Claver & Hoessel (2002), (iii) Liu & Di Stefano (2008) and (iv) Karachentsev et al. (2002). [c]observed X-ray luminosity (0.3–10.0 keV) based on the DKBBFTH model (see later). Numbers shown in superscript relate to the following references for source names: [1]SRW06, [2]Stobbart et al. (2004), [3]Read, Ponman & Strickland (1997), [4]Schlegel, Barrett & Singh (1997), [5]Grimm et al. (2005), [6]Liu & Mirabel (2005), [7]Feng & Kaaret (2005), [8]Colbert & Ptak (2002), [9]Liu & Bregman (2005), [10]Roberts & Warwick (2000), [11]Roberts et al. (2004), [12]Swartz et al. (2004), [13]Schlegel & Pannuti (2003), [14]Radecke (1997), [15]Immler & Wang (2001), [16]Vogler, Pietsch & Bertoldi (1997) and [17]Kaaret et al. (2003).

2 SOURCE SELECTION

Following the example of SRW06, we aim to use only the highest quality data publicly available from the *XMM–Newton* Science archive (XSA[3]) in order to provide the best characterization of the structure of ULX spectra. We therefore choose only the best data sets, ULX observations with $\gtrsim$10 000 accumulated EPIC counts ($\gtrsim$500 independent spectral bins available for fitting). This restriction is imposed based on the work of SRW06, whose analysis shows that this is a reasonable threshold for statistically distinguishing between physically motivated models, particularly above 2 keV. This constraint provides a sample of 12 sources, which are listed in Table 1. We note that this may not be an exhaustive list, but that the number of sources in our sample is probably sufficient to allow global trends to become apparent. Some of this sample of ULXs have been observed on more than one occasion, in which case we select the longest individual exposure to provide the clearest view of their spectrum. The selected ULXs all reside within nearby galaxies ($\lesssim$10 Mpc) due to restrictions enforced by data quality, and vary in foreground Galactic absorption in the range 1.39–31.1 $\times$ 10^{20} cm^{-2}. Their X-ray luminosities are representative of the full ULX range, $\sim$$10^{39}$ to a few 10^{40} erg s^{-1}.

3 OBSERVATIONS AND DATA REDUCTION

Data from the longest individual observation of each source in our sample were downloaded from the XSA. The data sets were reduced using standard tools in *XMM–Newton* SAS software (version 7.0.0).[4] We found that background flaring was severe enough in three cases that periods of data were lost, resulting in multiple exposure data sets within the same observation. Such flaring events took place during the observations of Holmberg II X-1 and M81 X-6 and

[3] See http://xmm.esac.esa.int/xsa/.

[4] See http://xmm.esac.esa.int/sas/.

Table 2. Observation details.

Source	Obs ID	Date	Off-axis angle[a] (arcmin)	Exp[b] (s)
NGC 55 ULX	0028740201	2001 November 14	4.2	30410
M33 X-8	0102640101	2000 August 04	0.4	8650
NGC 1313 X-1	0405090101	2006 October 15	0.8	90200
NGC 1313 X-2	0405090101	2006 October 15	6.2	90200
IC 342 X-1	0206890201	2004 August 17	3.6	19750
NGC 2403 X-1	0164560901	2004 September 12	5.4	58470
Ho II X-1	0200470101	2004 April 15	0.3	40800
M81 X-6	0111800101	2001 April 22	3.2	88300
Ho IX X-1	0200980101	2004 September 26	0.3	80400
NGC 4559 X-1	0152170501	2003 May 27	0.3	38300
NGC 5204 X-1	0405690201	2006 November 19	0.2	33700
NGC 5408 X-1	0302900101	2006 January 13	0.2	99300

Note. [a]Off-axis angle of source in the *XMM–Newton* EPIC field of view; [b]sum of GTIs for each observation (taken from pn data), calculated as per in the text.

Table 3. Size of regions used to extract the spectral data, and details of the resultant spectra.

Source	Extraction radius (arcsec)		Spectral bins[a]	Rate[b] (counts s^{-1})
	Source	Background		
NGC 55 ULX	34	51	884	2.13
M33 X-8	50	75	1252	9.56
NGC 1313 X-1	40	60	1616	1.19
NGC 1313 X-2	40*	60	1600	1.04
IC 342 X-1	36	54	516	0.68
NGC 2403 X-1	35	52.5	843	0.48
Ho II X-1	52	78	1358	4.93
M81 X-6	22	33	989	0.69
Ho IX X-1	42	63	2139	2.49
NGC 4559 X-1	34	51	593	0.50
NGC 5204 X-1	40	60	873	1.55
NGC 5408 X-1	40	60	990	1.42

Note. [a]Number of spectral bins available for fitting from combined EPIC detectors; [b]combined EPIC count rate of source during observation in the 0.3–10 kev band. *Alternative extraction region used in MOS1 because source positioned on edge of chip gap.

caused multiple exposures in the MOS detectors only. In each case, we find that one of the MOS exposures was heavily contaminated, so for these objects we only use the other MOS data, together with the pn data. The third observation to be affected in this way is that of M33 X-8. In this case, we find that the pn data are split into two exposures, whilst data from the MOS detectors are split into three exposures. The first exposure from each detector contains no usable information. On further examination, we find that the second MOS exposure is heavily contaminated by flaring, we therefore only use the second pn and third MOS exposures for the observation of this object. To remove any remaining flaring events from our observations, we constructed good time interval (GTI) files from pn data using a full-field 10–15 keV background light curve and count rate criteria. The exact value of the count rate criteria used to construct the source GTI files varies according to the field (typically excluding count rates higher than $\sim$1–1.5 counts s^{-1}) to provide the longest exposure whilst minimizing contamination. Details of these observations are included in Table 2, with listed exposure times incorporating the GTI corrections used during the reduction of the data.

The source spectra were extracted from circular apertures centred on the individual ULX in each detector. This was straightforward for the majority of data, but we found that NGC 1313 X-2 was unfortunately positioned on the chip gap of the MOS1 detector so a polygonal source region was applied to optimize our data extraction. Background spectra were obtained from larger circular regions placed near to the source. Where possible, these were positioned on the same chip and at a similar distance from the read-out node as the source. The only exception was NGC 4559 X-1, where the MOS detectors were operating in small window mode, therefore alternative background regions were selected on a separate chip in a position as close as possible to that used in the pn detector, whilst in the case of M81 X-6 no data were contained in the MOS1 observation. The size of the individual source and background extraction regions is recorded in Table 3 (in the case of NGC 1313 X-2, we only list the size of the circular apertures used in pn and MOS2).

The best quality data (FLAG = 0) were extracted in each case with PATTERN $\leq$ 4 for pn and PATTERN $\leq$ 12 for MOS. The response and ancillary response files were created automatically by the standard *XMM–Newton* tasks and spectral files were grouped to a minimum of 20 counts per bin to improve statistics. The number of independent spectral bins after this process was completed is listed in Table 3, along with the combined EPIC source count rates.

4 ULX SPECTRAL PROPERTIES

Our aims in this work are twofold. First, we aim to investigate the basic shape of the ULX X-ray spectra, and in doing so evaluate the evidence for the presence of a soft excess and a power-law break (at energies of a few keV) in ULX spectra. As these have been suggested as the two distinguishing spectral features of a new, ultraluminous accretion state (Roberts 2007), it is important to examine the evidence for their presence in the highest quality ULX spectra offered by *XMM–Newton*, and so determine the validity of claims of a new accretion state. Secondly, we will investigate the physical insights that a range of models can afford us on the nature of the accretion flows in this putative state. The models we use vary from the simplest empirical models (power-law continua), through accretion disc models, to models in which we consider both an accretion disc and a Comptonizing corona surrounding its inner regions, and the interplay between the two.

All spectra are fit in XSPEC version 11.3.2 over the 0.3–10.0 keV energy range (unless otherwise stated). To maximize data quality, pn and MOS data were fit simultaneously, with the addition of a constant multiplicative factor to compensate for calibration difference between the cameras. The pn constant is fixed at unity, whilst those for each MOS camera remain free, with the fitted values generally agreeing to within $\sim$10 per cent (larger discrepancies only occurred with disparate extraction regions; see Section 3 above for more details). In each case, the spectra are fit with two absorption components; one fixed at the column observed along the line of sight within our own Galaxy as listed in Table 1 (from Dickey & Lockman 1990), and a second component that is allowed to vary to represent any absorption within the host galaxy and/or intrinsic to the ULX. The absorption columns are modelled using the TBABS model (Wilms, Allen & McCray 2000). All quoted errors are the 90 per cent confidence interval for one interesting parameter.

Table 4. Simple power-law continuum and MCD spectral fits.

Source	Model parameters		χ^2/d.o.f.†
TBABS*TBABS*PO	$N_{\rm H}$ [a]	Γ[b]	
NGC 55 ULX	0.455 ± 0.008	3.30 ± 0.03	1288.8/879
M33 X-8	0.249*	2.218*	2527.3/1247
NGC 1313 X-1	0.188 ± 0.005	1.85 ± 0.02	2138.5/1611
NGC 1313 X-2	0.341 ± 0.008	1.81 ± 0.02	1982.4/1595
IC 342 X-1	0.57 ± 0.04	1.83 ± 0.05	534.3/511
NGC 2403 X-1	0.51 ± 0.02	2.38 ± 0.03	1247.3/838
Ho II X-1	0.158 ± 0.003	2.63 ± 0.01	1602.6/1363
M81 X-6	0.39 ± 0.01	2.09 ± 0.02	1825.9/985
Ho IX X-1	0.105 ± 0.003	$1.606^{+0.01}_{-0.009}$	2863.4/2112
NGC 4559 X-1	0.120 ± 0.009	2.29 ± 0.04	586.5/588
NGC 5204 X-1	0.153 ± 0.006	2.52 ± 0.03	986.3/868
NGC 5408 X-1	$0.091^{+0.004}_{-0.003}$	3.12 ± 0.02	1801.9/985
TBABS*TBABS *DISKBB	$N_{\rm H}$[a]	$kT_{\rm in}$[c]	
NGC 55 ULX	0.123*	0.573*	2067.2/879
M33 X-8	0.007 ± 0.003	1.11 ± 0.01	1470.7/1247
NGC 1313 X-1	0.008*	1.420*	5531.5/1611
NGC 1313 X-2	0.115 ± 0.004	1.53 ± 0.02	2091.5/1595
IC 342 X-1	0.19 ± 0.02	$1.75^{+0.07}_{-0.06}$	775.1/511
NGC 2403 X-1	$0.168^{+0.01}_{-0.009}$	1.06 ± 0.02	891.0/838
Ho II X-1	0.0*	0.580*	8242.0/1363
M81 X-6	0.111 ± 0.006	1.31 ± 0.02	1210.1/985
Ho IX X-1	0.0*	1.624*	9164.3/2112
NGC 4559 X-1	0.0*	0.708*	1545.6/588
NGC 5204 X-1	0.0*	0.618*	2533.2/868
NGC 5408 X-1	0.0*	0.314*	8294.8/985

Note. Model is abbreviated to XSPECsyntax: TBABS – absorption components for both Galactic and external absorption; PO – power law; DISKBB – MCD. Specific notes: [a]external absorption column ($\times 10^{22}$ cm^{-2}) left free during fitting, Galactic columns listed in Table 1; [b]power-law photon index; [c]inner-disc temperature (keV). *Best-fitting models to these data give a reduced χ^2 greater than 2, hence we do not place constraints due to the paucity of the fit. †Here and elsewhere we use 'd.o.f.' to abbreviate the number of degrees of freedom available when fitting a model.

4.1 Single-component phenomenological models

Simple, single-component models have been used rather successfully to describe the featureless spectra of ULXs in the low-to-moderate-quality data regime for some years (e.g. Humphrey et al. 2003; Swartz et al. 2004; Feng & Kaaret 2005; Winter, Mushotzky & Reynolds 2006). Here, we use only the highest quality data to perform our analysis, yet we still find the X-ray spectra of these objects to appear relatively smooth and featureless. Therefore, the application of these simple, single-continuum models is a good starting point in their analysis. We start by applying an absorbed power-law continuum (PO in XSPEC syntax) and an absorbed multicoloured disc blackbody (MCD) component (DISKBB in XSPEC ; Mitsuda et al. 1984) separately to the data. The resultant fits can be seen in Table 4.

Table 4 shows that a single power law is not a particularly good fit to ULX data of this high quality. Although a rough representation of the observed spectra (reduced χ^2, $\chi^2_\nu < 2$) is found for 11/12 objects, only two objects provide statistically acceptable fits (null hypothesis probability >5 per cent). Notably, these two objects – IC 342 X-1 and NGC 4559 X-1 – also have the worst quality data in the sample. The vast majority of the other ULX data reject this model at very high significance. The situation is even worse when fitting the MCD model, as seen in Fig. 1, where the quality of the fits is so bad they can only roughly represent five of the 12 spectra, and only one data set (NGC 2403 X-1) does not reject this model at high significance.

None the less, it is instructive to compare the parameters derived from these fits, since lower quality data would not be able to show the inadequacy of these models. For the spectra that are best represented by an absorbed MCD (again using the $\chi^2_\nu < 2$ criterion), we find that $kT_{\rm in} \sim 1.06$–1.7 keV. These are close to those seen in high-mass accretion rate Galactic sources in the high/soft (thermal-dominated) state (e.g. McClintock & Remillard 2006), which if taken at face value would indicate that the ULXs contain standard stellar mass black holes accreting at fairly high-mass accretion rates. Conversely, with a power-law model, Table 4 shows that the photon index measured when these objects are represented by an absorbed power-law range from $1.6 < \Gamma < 3.3$. While the steepest spectra would correspond to the very high (steep power-law) state, those with $\Gamma < 2.1$ correspond instead to the low/hard state (McClintock & Remillard 2006). The low/hard state is only seen at very sub-Eddington mass accretion rates ($<0.1 L/L_{\rm Edd}$), so a naïve interpretation of this spectral decomposition suggests that we are observing at least some IMBHs.

Clearly, the fits from these models contradict one another as individual ULX cannot be both stellar and IMBH – we note that the ULX data that are best represented by MCD fits generally also fit with power-law continua with $\Gamma < 2.3$. It is therefore evident that problems can arise when we attempt to draw physical meaning from simple phenomenological models applied to ULX data. In the case of the observations in our sample, we have sufficient data quality to demonstrate that the underlying spectrum is more complex than either standard disc or power-law models. As we have no reason to think our ULX sample is atypical of the class, then by extension this should apply to all ULXs, if sufficient data were available for them. This should render any physical conclusions drawn from simple model fits to low-to-moderate-quality ULX data as suspicious.

Single-component phenomenological models do not provide enough flexibility in fitting to accurately constrain the majority of the data, nor do they consistently provide a physically realistic basis on which to interpret the data. As our next step, we therefore turn to more complex phenomenological models that have been used to characterize the spectra of BHBs and ULXs.

4.2 Combined phenomenological models

Here, we combine the two simplest continuum models to further characterize the spectral shape and features of these sources. This combination of a disc component plus a power law has been used extremely effectively in BHBs (McClintock & Remillard 2006 and references therein), since although these models are not terribly physical, they provide a good approximation to a disc with an optically thin Comptonizing corona over the 3–20 keV range. It has also, of course, been used as the basis for claims of IMBHs underlying ULXs (see the Introduction). Each source spectrum is initially fit by an absorbed power-law component, then a multicoloured disc component is added to this to look for any improvement of fit. The results of these fits can be seen in Table 5.

Fig. 2 illustrates the need for a second spectral component in ULX spectra. Here, we see the spectrum of NGC 5408 X-1 deconvolved with the best-fitting absorbed MCD plus power-law model. It is clear from these data that a soft component is present in the spectrum, as an excess above a harder continuum. In fact, we find that all our sources show a significant improvement in χ^2 with the addition of a disc component (Table 5). This implies that some form of soft excess is ubiquitous in ULX spectra at this level of data quality.

Interestingly, in only 7/12 cases is the resulting disc 'cool', i.e. with $kT_{\rm in} < 0.4$ keV as in Miller et al. (2004). Instead we find

Table 5. Combined power law plus MCD spectral fits.

Source	TBABS*TBABS*(PO+DISKBB)				$\Delta\chi^{2d}$
	$N_{\rm H}{}^a$	Γ^b	$kT_{\rm in}{}^c$	χ^2/d.o.f.	
NGC 55 ULX	0.46 ± 0.02	3.7 ± 0.1	$0.77^{+0.03}_{-0.04}$	1042.7/877	246.06
M33 X-8	0.09 ± 0.02	2.0 ± 0.1	$1.05^{+0.03}_{-0.04}$	1216.0/1245	1311.30
NGC 1313 X-1	$0.26^{+0.02}_{-0.01}$	$1.70^{+0.03}_{-0.02}$	0.23 ± 0.01	1796.5/1609	341.88
NGC 1313 X-2	$0.29^{+0.03}_{-0.02}$	$2.0^{+0.2}_{-0.1}$	1.7 ± 0.1	1599.7/1593	382.77
IC 342 X-1	$0.7^{+0.2}_{-0.1}$	1.7 ± 0.1	$0.32^{+0.1}_{-0.09}$	518.0/509	16.29
NGC 2403 X-1	$0.38^{+0.08}_{-0.07}$	$2.9^{+0.3}_{-0.4}$	$1.12^{+0.04}_{-0.05}$	853.7/836	393.69
Ho II X-1	0.116 ± 0.007	2.42 ± 0.04	0.37 ± 0.02	1503.9/1361	98.71
M81 X6	$0.30^{+0.05}_{-0.04}$	$2.6^{+0.4}_{-0.3}$	$1.42^{+0.04}_{-0.05}$	1093.9/983	732.01
Ho IX X-1	0.135 ± 0.007	1.46 ± 0.02	$0.27^{+0.02}_{-0.01}$	2440.0/2110	423.44
NGC 4559 X-1	$0.16^{+0.03}_{-0.02}$	$2.14^{+0.07}_{-0.05}$	0.17 ± 0.02	528.1/586	58.36
NGC 5204 X-1	0.09 ± 0.01	$2.18^{+0.08}_{-0.09}$	0.39 ± 0.02	925.1/866	61.16
NGC 5408 X-1	$0.068^{+0.005}_{-0.006}$	2.68 ± 0.04	$0.186^{+0.007}_{-0.003}$	1320.5/983	481.41

Note. Models are abbreviated XSPECsyntax, as per Table 4. Specific notes: [a]external absorption column in units of 10^{22} atoms cm^{-2}; [b]power-law photon index; [c]inner-disc temperature (keV); [d]χ^2 improvement over the absorbed power-law fit (see Table 4), for two extra degrees of freedom.

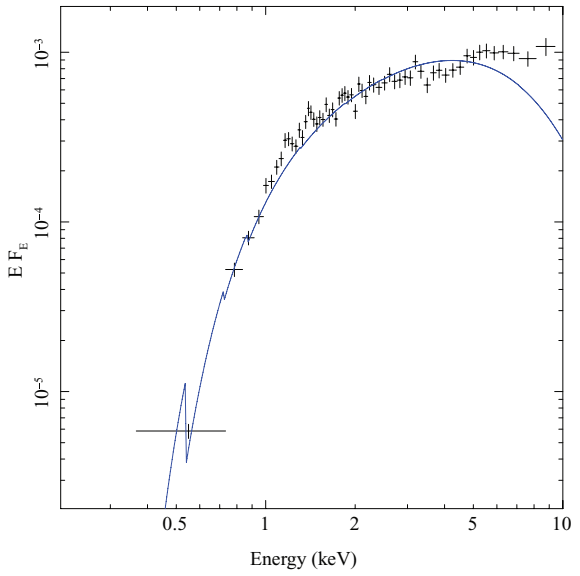

Figure 1. *XMM–Newton* EPIC pn data from IC 342 X-1 fit with an absorbed multicolour disc model (DISKBB). We plot only the pn data, shown in black, which we rebin to a minimum of 10σ statistical significance, or 10 channels per data point for clarity. Although this is statistically one of the better fits to an MCD model within our sample, a visual inspection quickly reveals the residuals (particularly evident at high energies) that explain why it is still rejected at high significance.

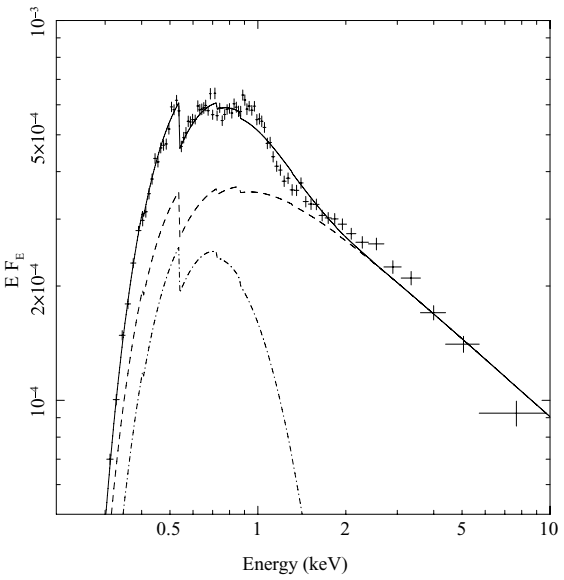

Figure 2. *XMM–Newton* EPIC pn data from NGC 5408 X-1 (black data points, rebinned to a minimum of 30σ significance or 30 channels), shown with the best-fitting multicolour disc plus power-law model (solid line). The contributions of the separate model components to the overall fit are overplotted as grey dashed (power-law continuum) and dash–dotted lines (MCD). This clearly shows the motivation for an additional soft component in the spectrum.

that the temperature from the disc component appears to vary over a much wider range, from $0.17 < kT_{\rm in} < 1.7$ keV, covering both the cool and standard disc temperature range. However, where the disc is hot – and so forms the predominant component at higher energies – we find that the power-law component contributes the soft excess, agreeing with previous work (e.g. Foschini et al. 2004; Stobbart, Roberts & Warwick 2004; Roberts et al. 2005). As with these analyses, we note that the power law extends to lower energies than its putative seed photons. This is not physically realistic and so requires more plausible physical modelling.

Inspection of the residuals from these fits also reveals a possible break or turnover above ∼2 keV. In some cases, this is also clearly visible in their spectra. We can see in Fig. 2 that the power-law cannot model such a feature and so is plotted in an average position, whilst the data curve around it. Such a feature is not present in standard BHB states and so deserves further investigation, which is carried out in the next section.

Another point worth noting is that the object with the highest inner-disc temperature is NGC 1313 X-2, an ULX that has exhibited much cooler disc temperatures in previous observations (e.g. 0.16 keV; Miller et al. 2003) leading to the suggestion that it harbours an IMBH. We note that a local minimum in χ^2 was observed at ∼0.16 keV in our data, but that the global minimum in our best fit occurs at much higher temperatures ($kT_{\rm in} = 1.7$ keV). It

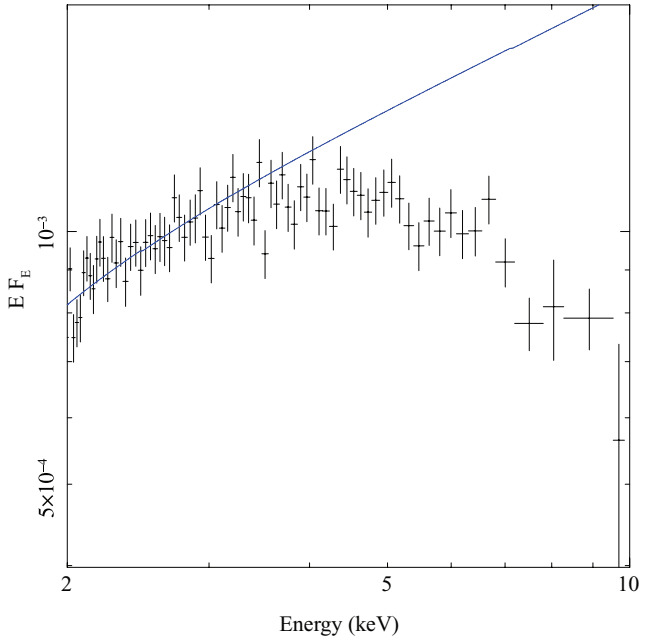

Figure 3. *XMM–Newton* EPIC pn data from NGC 1313 X-2, displayed as per previous figures (rebinned to a minimum of 15σ, or 15 channels). We show the data fit by a power-law component based on the slope and normalization of the low-energy (pre-break) component of the broken power-law fit to these data. It is very clear from these data that some form of break or curvature is present above 2 keV.

is clear that these results are contradictory – NGC 1313 X-2 cannot change from an IMBH to a stellar mass BHB between observations – demonstrating yet again that drawing physical conclusions from this soft component can be hazardous and should therefore be approached with care.

4.3 A high-energy break

We investigate the prevalence of a high-energy downturn following the analysis of SRW06, i.e. by comparing a power-law and a broken power-law description of the data above 2 keV. We do not include absorption in these fits as it is not easily constrained by data above 2 keV, and besides the wider band fits infer columns that have little effect above 2 keV. The resulting fits are shown in Table 6.

The broken power law is clearly visible in Fig. 3, and statistically preferred (>98 per cent significance improvement in fit according to the F-test) in 11 out of the 12 ULXs in our sample, with break energies in the ∼3.5–7 keV range, and a typical steepening of the power-law slope by $\Delta\Gamma \sim 1$–2. This near ubiquity is made all the more remarkable when it is considered that the one ULX without evidence for a break here – NGC 5204 X-1 – has displayed evidence for such a feature in previous observations (Roberts et al. 2005, SRW06). While this break is clearly expected from the 'hot disc' fits, where the MCD component dominates at high energies, the break is also seen at high significance in the 'cool disc' objects. These are the sources where the IMBH model is apparently favoured, implying that these ULXs are analogous to the low/hard state observed in Galactic BHBs. Yet, the high-energy data show a break at ∼5 keV which is not seen in this accretion state. The ubiquity of the high-energy break shows that the ULX spectra are *not* well described by a cool disc plus power law as expected from the IMBH model.

Instead, these high-quality data show that the disc is either hot, implying a stellar mass black hole (which must be accreting at or above Eddington in order to produce the observed luminosity) but with a previously unseen soft excess (an alternative would be that the power law is simple broadening the disc spectrum to explain a known state; see later for more detailed discussions), or cool but with a high-energy tail which is quite unlike that seen in the standard spectral states of BHBs (e.g. McClintock & Remillard 2006). This new combination of observational characteristics – a cool disc and a broken harder component – suggests that these ULXs are operating in an accretion state not commonly seen in the Galactic BHBs. We term this new combination of observational characteristics the 'ultraluminous state', and it seems most straightforward to assume that this state accompanies extremely high accretion rates on to stellar remnant black holes. As we also have no reason to think our ULX sample atypical of the class as a whole, we can only presume that this spectrum may be endemic to the majority of ULXs.

Table 6. A comparison of power-law to broken power-law spectral fits in the 2–10 keV band.

Source	PO		BKNPOWER				$\Delta\chi^{2e}$	1-P(F-test)^f
	Γ^a	χ^2/d.o.f.	$\Gamma_1{}^b$	$E_{\rm break}{}^c$	$\Gamma_2{}^d$	χ^2/d.o.f.		
NGC 55 ULX	3.57 ± 0.06	429.8/314	3.1 ± 0.1	3.9 ± 0.3	$4.9^{+0.5}_{-0.4}$	323.1/311	106.7	>99
M33 X-8	2.60 ± 0.03	855.6/679	$2.17^{+0.08}_{-0.1}$	$4.0^{+0.2}_{-0.3}$	3.4 ± 0.2	641.6/677	214.0	>99
NGC 1313 X-1	1.06 ± 0.02	1054.2/1043	$1.60^{+0.03}_{-0.05}$	$6.3^{+0.3}_{-0.9}$	$2.6^{+0.3}_{-0.5}$	992.9/1041	61.3	>99
NGC 1313 X-2	1.91 ± 0.02	1195.8/1034	$1.53^{+0.1}_{-0.07}$	$3.7^{+0.7}_{-0.2}$	$2.3^{+0.2}_{-0.1}$	1011.0/1032	184.8	>99
IC 342 X-1	$1.58^{+0.06}_{-0.05}$	281.3/269	1.53 ± 0.07	$6.7^{+0.7}_{-1.0}$	$2.7^{+1}_{-0.8}$	273.7/267	7.6	>99
NGC 2403 X-1	$2.67^{+0.05}_{-0.06}$	478.1/335	2.1 ± 0.1	4.0 ± 0.2	4.0 ± 0.3	335.0/333	147.1	>99
Ho II X-1	$2.58^{+0.02}_{-0.03}$	772.7/795	2.51 ± 0.04	$5.4^{+0.5}_{-0.6}$	$3.1^{+0.3}_{-0.2}$	750.5/793	22.2	>99
M81 X-6	2.31 ± 0.03	903.9/538	$1.72^{+0.07}_{-0.1}$	4.1 ± 0.2	3.4 ± 0.2	554.9/536	349.0	100
Ho IX X-1	1.46 ± 0.02	1672.6/1544	1.38 ± 0.02	$6.2^{+0.3}_{-0.4}$	2.2 ± 0.2	1561.1/1542	111.5	>99
NGC 4559 X-1	$2.22^{+0.07}_{-0.09}$	141.1/153	2.1 ± 0.1	$4.8^{+1}_{-0.9}$	$2.8^{+0.8}_{-0.4}$	133.8/151	7.3	98.1
NGC 5204 X-1	2.40 ± 0.06	319.5/307	$2.36^{+0.09}_{-0.2}$	5^{+3}_{-2}	$2.7^{+2}_{-0.5}$	316.7/305	2.8	73.9
NGC 5408 X-1	$2.84^{+0.04}_{-0.06}$	442.0/417	2.80 ± 0.06	$7.1^{+1}_{-0.9}$	7^{+7}_{-2}	432.4/415	9.6	98.9

Note. Models are abbreviated to XSPECsyntax: PO – as before; BKPOWER – broken power-law model. Specific notes: [a]photon index from PO model, [b]photon index before the break in BKNPOWER model, [c]break energy (keV), [d]photon index after the break energy, [e]χ^2 improvement over a single power-law fit, [f]statistical probability (in per cent) that the broken power-law model provides an improvement to the fit over a single PO model, from the F-test.

4.4 More physical models: slim disc

The investigations and results described above have focused on the application of simple phenomenological models used to characterize the shape of the observed spectra of these sources. This work has revealed the presence of both a soft excess and a break above ∼2 keV. These studies have also shown the limitations of these models at this level of data quality, especially the MCD fits. Disc spectra should be more complex than this simple sum-of-blackbody approach. First, relativistic effects broaden the spectrum, so it is less strongly peaked than an MCD (Cunningham 1975; Ebisawa et al. 2001; Li et al. 2005). Secondly, the intrinsic spectrum from material at a given radius is not a true blackbody as there is not enough absorption opacity to thermalize the emission at all energies (Davis et al. 2005). This can be approximated by a colour temperature correction (Shimura & Takahara 1995), but this is only an approximation and the best current models of disc spectra show weak atomic features in the continuum emission. Hence, even relativistic, colour-corrected blackbody discs are not an accurate description of the best theoretical disc spectra over the 0.3–10 keV band pass, though they are normally an excellent fit to the 3–20 keV energy range (Done & Davis 2008). This can be seen in real data from disc-dominated BHB systems, for example the 0.3–10 keV spectrum from Large Magellanic Cloud X–3 is better fit by full-disc models than by DISKBB (Davis, Done & Blaes 2006). However, only a few ULXs fit well even to these full-disc models (Hui & Krolik 2008).

These models also assume that advection of radiation is not important, yet in ULXs we may be observing a super-Eddington accretion flow. The disc becomes so optically thick at these extreme mass accretion rates that the energy released in the mid-plane of the disc does not have time to diffuse to the photosphere. Instead, the photons are carried along with the inflowing material, being advected radially rather than being radiated vertically (Abramowicz et al. 1988). Such radiatively inefficient, optically thick, advection-dominated disc solutions (termed 'slim discs') are physically very different to the optically thin, advection-dominated flows (ADAFs) of Narayan & Yi (1995), as the energy is advected in photons rather than in protons. The additional cooling from advected photons is most important in the inner regions of the disc, so the expected luminosity from each disc radius of the slim disc is progressively lower than that of a standard accretion disc at the same mass accretion rate (Abramowicz et al. 1988). Thus, these models predict that the slim-disc spectra are less sharply curved than that of a standard disc, so these generally give a better fit to the data. Additionally, the slim discs may extend down to smaller radii than the classic last stable orbit due to the non-negligible pressure support, so their spectra can include higher temperature components than expected from a standard disc (Abramowicz et al. 1988; Watarai et al. 2000, but see also Beloborodov 1998). Such high-temperature components, if interpreted as emission from a standard accretion disc, would give an underestimate of the black hole mass (e.g. Makishima et al. 2000).

To take these physical differences into account, we replace the standard MCD model with a modified version, the 'p-free' disc model. This allows the disc temperature to scale as r^{-p}, where r is the radius and p is a free parameter. Standard (MCD) discs have p fixed at 0.75, but increasing amounts of advection can be modelled by decreasing p, with fully advective discs having $p \simeq 0.5$ (e.g. Watarai, Mizuno & Mineshige 2001; Miyawaki et al. 2006; Vierdayanti et al. 2006). Hence, a p-free disc fitting with $p \sim 0.5$ would be indicative of the slim-disc model, and also gives a broader spectrum which can approximate the effects of the relativistic effects and colour temperature correction.

The p-free model gives a slightly better overall fit to the data than a single power law, with all ULXs being at least roughly represented with this gentle spectral curvature. Indeed, five out of 12 ULXs have statistically acceptable fits to this model. If we consider the values derived from best fits to the data we find, at first glance, that our results appear to be in good agreement with the slim-disc model, with $p \sim 0.4$–0.6 (see Table 7), but on closer inspection problems begin to emerge. Table 7 shows that while some of the derived inner-disc temperatures are in the 1–3 keV range expected for such super-Eddington flows on to stellar mass black holes, some are extremely high, with four of the 12 sources providing fits above 6 keV (including two of the acceptable fits). Such temperatures are high even for maximally spinning black holes

Table 7. Spectral fits for the p-free disc model.

Source	TBABS*TBABS*DISKPBB			
	$N_{\rm H}$ [a]	$T_{\rm in}$ [b]	p [c]	χ^2/d.o.f.
NGC 55 ULX	0.38 ± 0.01	$1.12^{+0.06}_{-0.05}$	0.408 ± 0.005	1019.9/878
M33 X-8	$0.090^{+0.009}_{-0.01}$	$1.36^{+0.03}_{-0.04}$	$0.599^{+0.01}_{-0.009}$	1242.0/1246
NGC 1313 X-1	$0.188^{+0.003}_{-0.005}$	7.9 ± 0.8	0.521 ± 0.002	2113.2/1610
NGC 1313 X-2	$0.251^{+0.009}_{-0.01}$	$2.31^{+0.09}_{-0.1}$	$0.583^{+0.009}_{-0.006}$	1601.2/1594
IC 342 X-1	0.57 ± 0.04	13^{+7}_{-4}	0.523 ± 0.007	532.1/510
NGC 2403 X-1	0.27 ± 0.03	1.24 ± 0.06	$0.60^{+0.03}_{-0.02}$	850.5/837
Ho II X-1	0.149 ± 0.003	$2.80^{+0.1}_{-0.10}$	0.436 ± 0.001	1557.0/1362
M81 X-6	$0.23^{+0.01}_{-0.02}$	$1.60^{+0.05}_{-0.06}$	$0.61^{+0.02}_{-0.01}$	1091.7/984
Ho IX X-1	0.103 ± 0.003	$8.9^{+2}_{-0.4}$	$0.557^{+0.001}_{-0.002}$	2853.2/2111
NGC 4559 X-1	$0.121^{+0.01}_{-0.009}$	$6.2^{+0.6}_{-0.8}$	$0.466^{+0.004}_{-0.002}$	574.7/587
NGC 5204 X-1	$0.147^{+0.007}_{-0.004}$	3.0 ± 0.2	$0.446^{+0.002}_{-0.003}$	977.5/867
NGC 5408 X-1	0.085 ± 0.004	$1.97^{+0.1}_{-0.05}$	0.392 ± 0.002	1855.5/984

Note. Model is abbreviated to XSPECsyntax: TBABS – absorption components for both Galactic and external absorption; DISKPBB – p-free disc. Specific notes: [a]external absorption column ($\times 10^{22}$ cm^{-2}) left free during fitting, Galactic columns listed in Table 1; [b]inner-disc temperature (keV); [c]p value, where disc temperature scales as r^{-p} and r is the radius.

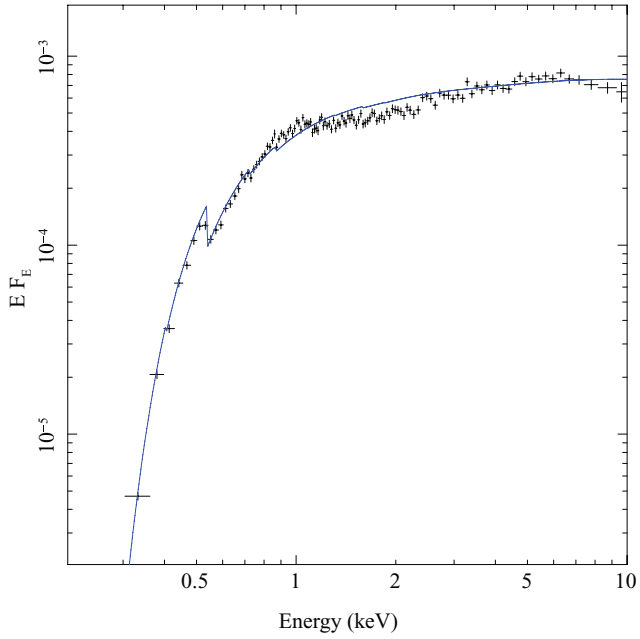

Figure 4. *XMM–Newton* data of NGC 1313 X-1, deconvolved with the '*p*-free' model. The data are plotted as per the previous figure, and binned to a minimum of 20σ or 20 channels for clarity. This model is used as a simplified description of the theoretically predicted 'slim-disc' model. Although the *p*-value ($p \sim 0.5$) for these data could be considered in support of a slim disc, the best fit provides an unrealistic disc temperature ($kT_{\rm in} \sim 7.9$ keV).

(Ebisawa et al. 2003), making these fits physically unrealistic. These high-quality data sets also clearly show that the spectral curvature is more complex in many cases, even for this modified disc model. One clear example of this is NGC 1313 X-1 (one of the unphysically high-temperature spectra) where there is a marked inflection present in the spectral data at ∼2 keV which cannot be matched in the *p*-free models (Fig. 4; this is also obvious in the spectra of several other ULXs, see Fig. 8). So, although a *p*-free model with slim-disc characteristics (or indeed a full standard disc model: Hui & Krolik 2008) cannot be ruled out in the minority of cases, it does not seem to be a good explanation for ULXs as a class. The two-component phenomenological model (MCD plus power law) is clearly a better statistical description of the majority of ULX spectra, though the presence of a high-energy break clearly also shows its limitations. As a next step, we replace the power law with a Comptonization model, to explore the nature of the high-energy break.

4.5 Comptonization models

We have demonstrated that the highest quality ULX data indicate that many of these objects are in a new, ultraluminous accretion state. The next, obvious question is: what are the physics of the accretion flow producing this shape of spectrum? In order to further explore the nature of these systems, we now replace the power-law continuum with more physically realistic Comptonization models. We use an alternative disc model, DISKPN (Gierliński et al. 1999), which incorporates an approximate stress-free inner boundary condition as opposed to the continuous stress assumed in DISKBB. The resulting spectra differ by less than 5 per cent for the same temperature, but we use DISKPN so as to be able to directly compare our results with those of SRW06.

4.5.1 DISKPN+COMPTT

We initially use COMPTT (Titarchuk 1994) to model the coronal emission. This is an analytic approximation to non-relativistic thermal Comptonization which assumes that the seed photons for Comptonization have a Wien spectrum. We tie the temperature of these seed photons to the temperature of the accretion disc ($T_{\rm max}$). In each case, the redshift is fixed at zero due to the proximity of these systems, whilst the optical depth and plasma temperature are free to vary. We show the results of our spectral fitting in Table 8.

We find in each case that there is a local minimum in χ^2 space which corresponds to a hot, optically thin Comptonizing corona ($kT_{\rm e} \sim 50$ keV, $\tau \lesssim 1$), similar in nature to that seen in Galactic BHBs in classic accretion states. However, the global minimum in χ^2 occurs for a fit that describes a cool, optically thick corona

Table 8. Application of Comptonization models: DISKPN+COMPTT spectral fits.

Source	TBABS*TBABS*(DISKPN+COMPTT)				χ^2/d.o.f.	$\Delta\chi^{2e}$	1-P(F-test)^f
	$N_{\rm H}{}^a$	$T_{\rm max}{}^b$	$kT_{\rm e}{}^c$	τ^d			
NGC 55 ULX	0.235 ± 0.004	$0.221^{+0.010}_{-0.006}$	$0.83^{+0.05}_{-0.04}$	9.9 ± 0.4	986.3/876	252.6	>99
M33 X-8	0.041 ± 0.003	$0.87^{+0.04}_{-0.2}$	$1.39^{+0.08}_{-0.03}$	80^{+100}_{-30}	1204.4/1244	42.2	>99
NGC 1313 X-1	0.21 ± 0.01	0.23 ± 0.01	2.1 ± 0.1	$8.5^{+0.6}_{-0.5}$	1705.7/1608	192.0	>99
NGC 1313 X-2	$0.195^{+0.004}_{-0.005}$	$0.7^{+0.2}_{-0.1}$	1.51 ± 0.02	$15.3^{+0.4}_{-1}$	1613.2/1592	281.6	>99
IC 342 X-1	$0.58^{+0.10}_{-0.1}$	$0.30^{+0.2}_{-0.08}$	$2.78^{+8}_{-0.6}$	7^{+3}_{-7}	515.5/508	4.4	87.5
NGC 2403 X-1	$0.18^{+0.06}_{-0.01}$	$0.27^{+0.1}_{-0.05}$	0.98 ± 0.04	12.5 ± 0.7	844.7/835	131.4	>99
Ho II X-1	0.033 ± 0.002	$0.23^{+0.02}_{-0.01}$	$2.12^{+0.1}_{-0.10}$	5.5 ± 0.2	1375.4/1360	44.2	>99
M81 X-6	0.181 ± 0.006	$0.7^{+0.1}_{-0.2}$	$1.15^{+0.02}_{-0.01}$	31^{+4}_{-3}	1082.7/982	56.8	>99
Ho IX X-1	0.099 ± 0.006	0.26 ± 0.02	$2.27^{+0.1}_{-0.09}$	9.5 ± 0.5	2284.2/2109	126.4	>99
NGC 4559 X-1	$0.13^{+0.03}_{-0.02}$	0.16 ± 0.02	$1.8^{+0.6}_{-0.3}$	$7.4^{+0.7}_{-1}$	513.1/585	32.4	>99
NGC 5204 X-1	$0.035^{+0.007}_{-0.009}$	0.26 ± 0.03	$2.2^{+2}_{-0.4}$	6^{+2}_{-3}	886.2/865	3.9	87.5
NGC 5408 X-1	0.029 ± 0.005	$0.170^{+0.006}_{-0.007}$	$1.5^{+0.3}_{-0.2}$	$6.5^{+0.8}_{-0.9}$	1240.9/982	41.1	>99

Note. Models are abbreviated to XSPECsyntax: DISKPN – accretion disc model, COMPTT – Comptonization model. Specific notes: [a]external absorption column in units of 10^{22} atoms cm^{-2}, [b]maximum temperature in the accretion disc (keV), [c]plasma temperature in the Comptonizing corona, [d]optical depth of corona, [e,f] χ^2 improvement and statistical probability (in per cent) of the fit improvement over a hot optically thin corona with $kT_{\rm e} = 50$ keV fixed.

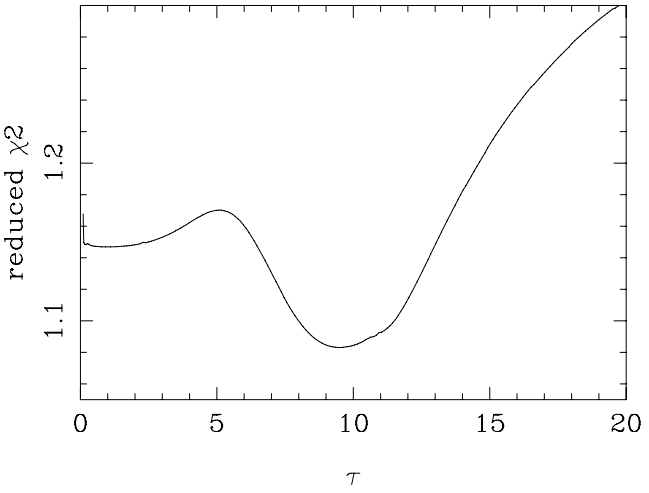

Figure 5. Variation in χ^2 over a range of optical depths derived from the fitting of an absorbed DISKPN plus COMPTT to the data from Ho IX X-1. A local minimum is observed at lower optical depths, but this clearly shows that the global minimum occurs at $\tau \sim 9.5$, an optically thick solution.

($kT_e \sim 1$–3 keV and $\tau \sim 6$–80). This is a very different scenario to those of the standard black hole accretion states. We illustrate this in Fig. 5, which shows χ^2 versus τ for Ho IX X-1. Here, we find that a local minimum is observed at low optical depths, but a clear global minimum occurs at $\tau \sim 9.5$, an optically thick solution.

To quantify this improvement, we have compared the fits achieved in each scenario and find that in 10 of the 12 spectra the improvement in χ^2 is highly significant ($\Delta\chi^2 > 30$) (see Table 8), while the other two still show $\Delta\chi^2 > 3.9$, i.e. the break is detected at 90 per cent significance. To test this further, we fix the temperature of the corona at 50 keV (all hot corona local minima fits lie at approximately this temperature within errors). We compare the resultant fits to those given in Table 8 using the F-test, finding that in 10 out of 12 cases in our sample shows a >99 per cent statistical probability of improvement when applying a cool optically thick corona over a hot optically thin one. The possible presence of such an extraordinary corona is therefore the first major clue as to the origin in the physical differences between sub-Eddington accretion states and the ultraluminous state.

A second characteristic found in fitting this model to our ULX data is that the disc temperatures are generally cool. In fact, Table 8 shows that 9/12 disc temperatures reside (on face value) in the IMBH range ($T_{max} < 0.5$ keV), while the remaining three objects have hotter discs that might imply stellar mass objects. Similar results – a combination of a cool disc and an optically thick cool Comptonizing corona – have been found in previous studies of individual sources (e.g. Ho IX X-1 by Dewangan, Griffiths & Rao 2006; Ho II X-1 in Goad et al. 2006; also SRW06). However, in interpreting the cool disc component we must consider the implications of the presence of an optically thick corona. It is likely that such a medium would mask the innermost radii of the disc. It is also likely that material and power may be drawn from the disc to feed the corona. A combination of these factors could greatly impact the observed temperature of the accretion disc, invalidating any conclusions drawn on this basis. We return to this point later.

4.5.2 *DISKPN+EQPAIR*

We now apply an alternative, more physically self-consistent Comptonization model to test our provisional result from the DISKPN+COMPTT model further. Here, we use EQPAIR (Coppi 1999), a model which allows both thermal and non-thermal electrons, and calculates the resulting spectrum without assuming that the electrons are non relativistic, and where the seed photons can have a disc or blackbody spectrum. We choose to use thermal electrons plus disc emission to allow for comparison to COMPTT, and again tie the temperature of the seed photons to that of the inner accretion disc.

Comparing the fits to the data for DISKPN+COMPTT (Table 8) with DISKPN+EQPAIR (Table 9), we find that similar χ^2 values are achieved in all cases. Results once again indicate that the global fitting minima are achieved by a relatively cool accretion disc ($0.18 < T_{max} < 0.63$ keV) with a cool optically thick corona ($\tau \sim 7.0$–27.6), thick enough to potentially hide the inner disc.

Table 9. Application of Comptonization models: DISKPN+EQPAIR spectral fits.

Source	TBABS*TBABS*(DISKPN+EQPAIR)				χ^2/d.o.f.
	$N_H{}^a$	$T_{max}{}^b$	$l_h/l_s{}^c$	τ^d	
NGC 55 ULX	$0.250^{+0.01}_{-0.004}$	$0.253^{+0.01}_{-0.005}$	1.24 ± 0.03	$26.9^{+0.7}_{-2}$	990.2/876
M33 X-8	$0.036^{+0.004}_{-0.005}$	0.63 ± 0.02	$0.70^{+0.03}_{-0.02}$	$13.2^{+0.5}_{-0.8}$	1204.0/1244
NGC 1313 X-1	$0.210^{+0.005}_{-0.01}$	$0.271^{+0.004}_{-0.010}$	4.02 ± 0.07	$17.9^{+0.5}_{-0.6}$	1711.6/1608
NGC 1313 X-2	0.204 ± 0.01	$0.37^{+0.02}_{-0.04}$	$2.28^{+0.05}_{-0.06}$	$17.7^{+0.6}_{-0.8}$	1601.8/1592
IC 342 X-1	$0.64^{+0.08}_{-0.07}$	$0.32^{+0.02}_{-0.05}$	$3.2^{+0.5}_{-0.1}$	$11^{+3}_{-0.3}$	516.1/508
NGC 2403 X-1	$0.24^{+0.04}_{-0.02}$	$0.32^{+0.04}_{-0.05}$	$1.87^{+0.05}_{-0.07}$	27.6 ± 2	849.3/835
Ho II X-1	$0.050^{+0.002}_{-0.001}$	$0.267^{+0.007}_{-0.003}$	$1.011^{+0.009}_{-0.01}$	7.00 ± 0.02	1391.2/1360
M81 X-6	$0.20^{+0.02}_{-0.03}$	$0.30^{+0.1}_{-0.02}$	$2.6^{+0.1}_{-0.6}$	25^{+3}_{-1}	1085.2/982
Ho IX X-1	$0.109^{+0.005}_{-0.004}$	$0.312^{+0.01}_{-0.006}$	4.99 ± 0.08	$18.5^{+0.4}_{-0.3}$	2293.1/2109
NGC 4559 X-1	$0.14^{+0.01}_{-0.02}$	0.177 ± 0.009	2.2 ± 0.1	14 ± 2	513.8/585
NGC 5204 X-1	0.047 ± 0.003	0.314 ± 0.01	$1.35^{+0.07}_{-0.05}$	10^{+1}_{-2}	894.3/865
NGC 5408 X-1	$0.033^{+0.002}_{-0.001}$	$0.184^{+0.003}_{-0.002}$	$1.140^{+0.02}_{-0.009}$	$12.9^{+0.4}_{-0.6}$	1244.2/982

Note. Models are abbreviated to XSPECsyntax: DISKPN – accretion disc model, EQPAIR – Comptonization model. Specific notes: [a]external absorption column in units of 10^{22} atoms cm^2, [b]maximum temperature in the accretion disc (keV), [c]ratio between the compactness of electron and the compactness of seed photon distribution, [d]optical depth.

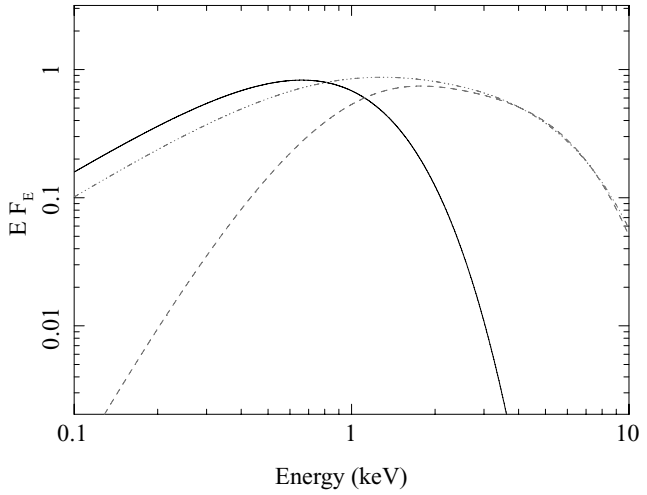

Figure 6. Comparison of disc plus Comptonization models used within our analysis. An average cool disc is plotted in black with coronal components representative of those found in our fits shown in grey (dashed line – COMPTT; dash–dotted line – EQPAIR). Although the Comptonization components have different spectral structures at lower energies, it is clear that the same cool optically thick corona is achieved at higher energies of the *XMM–Newton* band pass. The differences that are evident in the lower part of our energy range are accounted for by the other components in our model.

Fig. 6 illustrates the similarity in results between the two Comptonization models. Here, we plot typical values from our fits for both Comptonization components in grey (COMPTT – dashed line; EQPAIR – dash–dotted line) along with an average disc shown in black. We can clearly see that each of these models exhibits similar curvature at higher energies. The difference in the spectrum of these coronal components lies at lower energies where subtle variations in the disc and absorption components can compensate for this. Each of these models can therefore explain the curvature observed at both higher and lower energies within our band pass. The soft excess at low energies is modelled well by a cool accretion disc, whilst the optically thick corona causes the downturn at high energies (irrespective of model choice).

When these results are compared to the findings of SRW06, we find that we achieve similar fits to the data.[5] Their results also indicate the presence of a cool accretion disc ($0.08 < kT_{\rm max} < 0.29$ keV) in all cases, whilst an optically thick corona is observed in almost all sources (τ ranges from 0.2–33). It is therefore clear that these appear to be the physical characteristics of ULXs, and hence the ultraluminous state. This clearly demonstrates that we appear to be observing a radically different accretion flow to the classic accretion states viewed in Galactic BHBs.

We should note, however, that there are at least two Galactic black hole candidates that exhibit similar (albeit less extreme) spectral traits when modelled similarly – an unusually cool accretion disc and a cool optically thick corona – to the ULXs observed within our sample (when band pass is considered). These objects are GRS 1915+105 and XTE J1550-564, and in each case these objects are thought to be accreting at, or above, the Eddington limit when displaying such traits (Kubota & Done 2004; Middleton et al. 2006; Ueda, Yamaoka & Remillard 2009). This is further evidence to support the assertion that the ultraluminous state represents a super-Eddington accretion flow.

[5] We have five data sets in common with SRW06, and a further four sources with improved data.

4.6 Energetic disc–corona coupling

We now move on to the final stage in our analysis to further explore the results provided by Comptonization models. The models above implicitly assume that we can still observe the disc down to its innermost stable orbit. This assumption requires that the optically thick corona does not intercept our line of sight to the inner disc and that the underlying disc spectrum is independent of that of the corona (see Kubota & Done 2004). Yet both assumptions are probably flawed. An optically thick corona could easily mask the innermost regions (depending on its geometry; Kubota & Done 2004). Secondly, we must consider the energetics of both components. Both the disc and the corona must be ultimately powered by gravitational energy release. If we are observing a powerful corona, this implies that less energy is available for heating the disc (Svensson & Zdziarski 1994). The only code currently available that enables us to explore the effect of relaxing these assumptions is DKBBFTH (Done & Kubota 2006). This was designed to model the extreme very high state spectra seen in BHBs, such as XTE J1550-564 and GRS 1915+105. It incorporates the energetic disc–corona coupling model of Svensson & Zdziarski (1994), which assumes that the corona extends over the inner disc from $R_{\rm in}$ to $R_{\rm T}$, taking a fraction f of the gravitational energy available at these radii. Only the remaining fraction $(1 - f)$ is available to power the inner-disc emission, so the inner disc is cooler, but more importantly, less luminous than it would be if the corona were not present. This distorted inner-disc spectrum is the source of seed photons for the Comptonization (Done & Kubota 2006).

This model has five free parameters (only one more than in the purely phenomenological MCD plus power-law model and the same as for all the disc plus Comptonization models). The first two are the temperature of the Comptonizing plasma, $kT_{\rm e}$, and its optical depth (parametrized by the asymptotic spectral index, Γ). The disc is assumed to extend to some inner radius, $R_{\rm in}$, which is given by the overall normalization of the model, and with a temperature distribution *in the limit of no corona being present* of $T(R)_0 = T_{\rm in}(R/R_{\rm in})^{-3/4}$, i.e. as in the DISKBB model. However, the model assumes that the corona extends homogeneously (constant temperature and optical depth) in a slab over the disc, from its inner radius to $R_{\rm T}$ (in units of the Schwarzschild radius, $R_{\rm s} = 2GM/c^2$). For all radii between this and $R_{\rm in}$, the calculated disc temperature is $T(R) = T(R)_0(1 - f)^{1/4}$, where f is the fraction of power dissipated in the corona (assumed constant with radius) which is self-consistently calculated via iteration from the coronal spectral parameters (Done & Kubota 2006). The resulting disc luminosity underneath the corona is reduced by a factor of $(1 - f)$, but only a fraction $e^{-\tau}$ of this is seen directly, with the remainder being Compton scattered by the corona (Done & Kubota 2006).

Despite being more physically constrained, the model gives an equivalently good fit to the data as the disc plus Comptonization models discussed above. Fig. 7 shows this fit for Ho IX X-1, with the outer (un-Comptonized) disc emission (red solid line) dominating at soft energies. The inner-disc emission (red dotted line) is much lower than in standard disc models as much of the energy is powering the corona. These form the seed photons for the Compton scattering, but since this scattering is in an optically thick corona, these photons are *not* seen as almost all of them are upscattered to form the Comptonized spectrum (solid green line).

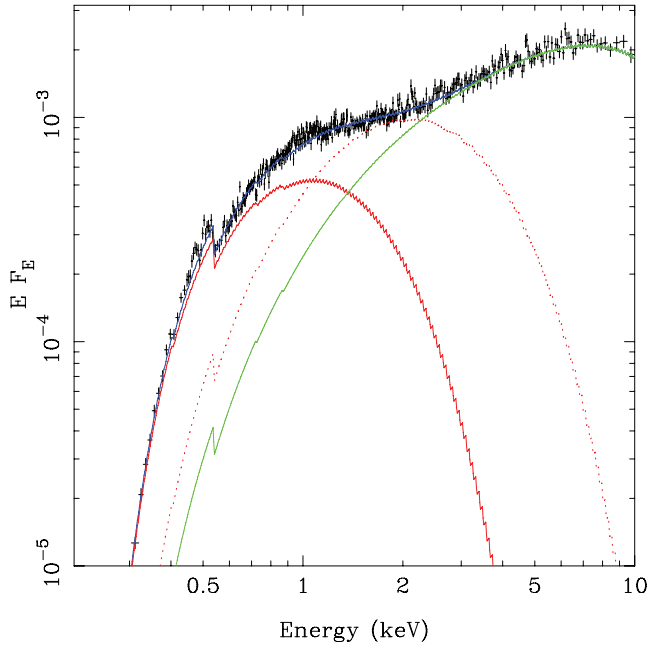

Figure 7. *XMM–Newton* EPIC pn data from Ho IX X-1 fit with an absorbed ultraluminous model (DKBBFTH, in blue). We plot only the pn data, shown in black, which we rebin to a minimum of 15σ significance or 15 channels for clarity. We also plot the various components of the accretion system described by the model; once again disc components are plotted in red whilst the corona is in green. The visible regions of the outer disc and the optically thick corona are plotted with a solid line, whilst the masked emission from the cooled, energetically coupled inner disc is represented by a dotted line. This shows that the curvature at lower energies is due to emission from the outer accretion disc (we are not able to directly observe emission from the innermost regions), and the break or turnover at higher energies is caused by the emission from the optically thick corona.

Fig. 8 shows the model fit to all our sources, with the pn data corrected for absorption to show the intrinsic spectral shape. This clearly shows the difficulties in interpreting the parameters from simple, phenomenological spectral fits. Again, using Ho IX X-1 as an example, the data have an inflection at soft energies that characterizes the soft excess. The characteristic energy of this feature is interpreted as the peak of the disc emission in the MCD plus power-law model (giving a very low temperature: hence IMBHs), while the high-energy break forms the peak of the disc temperature in single-component disc models (giving a very high temperature: too extreme even for stellar mass black holes). In these coupled disc–corona models, the 'true' disc temperature is not given by either of these observed features! The high-energy break is from the very low plasma temperature of the Comptonizing region, while the low-energy inflection occurs when the outer, un-Comptonized disc emission starts to dominate the spectrum. The inferred intrinsic inner-disc temperatures, recovered from the assumption of disc–corona energy partition, range from $0.3 < kT_{\rm disc} < 1.2$ keV with 8/12 giving fits where $kT_{\rm disc} > 0.5$ keV, which lies in the stellar mass black hole regime. This can be seen explicitly by converting the inferred inner radius into black hole mass assuming that the disc extends down to the last stable orbit around a Schwarzschild black hole at $R_{\rm in} = 6GM/c^2 = 8.9M$. All these 'hot' ULXs ($kT_{\rm disc} > 0.5$ keV) have inferred black hole masses $<100\,{\rm M}_{\odot}$, consistent with stellar mass black holes, and consequently derived $L_X/L_{\rm Edd} \gtrsim 1$.

However, a third of these source spectra are best fit by $kT_{\rm disc} < 0.5$ keV, hence giving black hole masses in the range 80–430 $\rm M_{\odot}$ and *sub*-Eddington accretion rates assuming that the disc extends down to the last stable orbit. We propose instead that this very cool temperature, and hence large radius, is *not* associated with the direct disc emission but instead arises as the accretion rate increases beyond that of standard super-Eddington accretion. In a supercritical accretion regime, the inner regions of the disc and corona may be blown off in the form of a wind, forming an optically thick photosphere out to large radii (e.g. Poutanen et al. 2007). We return to this point in the next section.

5 DISCUSSION: ULTRALUMINOUS X-RAY SOURCES, SUPER-EDDINGTON ACCRETION AND THE ULTRALUMINOUS STATE

We have examined 12 of the highest quality ULX data sets currently available in the public archives of the *XMM–Newton* telescope. Initial characterization of the spectrum of these sources reveals the presence of both a soft excess and a break at higher energies (within the *XMM–Newton* band pass). The existence of curvature at lower energies is apparent in many of the standard BHB accretion states, and is regularly fit by an accretion disc (Done, Gierliński & Kubota 2007). It is this standard practice which led to the suggestion that these objects were IMBHs, due to the low temperature of the apparent disc emission.

However, the detection of a break or curvature at higher energies (∼5 keV) brings new insights. Such a feature has been observed in ULXs previously (e.g. Foschini et al. 2004; Feng & Kaaret 2005; SRW06; Miyawaki et al. 2009), but here we show that it is nearly ubiquitous in the highest quality spectral data, with $\gtrsim$ 10,000 counts. No such break at these low energies is observed in the high-energy tail of any of the standard accretion states observed in BHBs (Remillard & McClintock 2006; Done et al. 2007),[6] so this challenges the basic assumption of the IMBH model, which is that we are observing standard accretion states that are scaled with the mass of the compact object. Thus, we must consider the alternative that we are observing a different accretion state than those generally seen in BHBs. A new accretion state would require us to be observing a different mass accretion rate with respect to Eddington than those seen in the standard states. Since these span (∼10^{-7} to 1) $L_{\rm Edd}$ (McClintock & Remillard 2006), then this is most likely a super-Eddington state, so requires a stellar mass rather than IMBH accretor.

We therefore suggest that a new observational state should be defined based on the characteristic signatures of ULXs. The ultraluminous state is one in which we observe a new combination of observational signatures; both a cool disc and a break or rollover at high energies in the band pass of the *XMM–Newton* telescope. We caution that high-quality data are required for a clear identification; the high-energy break in particular is difficult to identify with less than ∼10 000 counts in the X-ray spectrum.

In order to explore the physical origins of this state, we applied more physically motivated models to the data. One theory that has been presented to explain such an accretion state is the 'slim-disc' model, where advection of radiation suppresses the emitted disc luminosity of the innermost regions (Abramowicz et al. 1988). We

[6] Whilst there is a break in the high-energy tail of the low/hard and very high states, it is at energies $\gtrsim$100 and 20–30 keV, respectively (cf. McClintock & Remillard 2006).

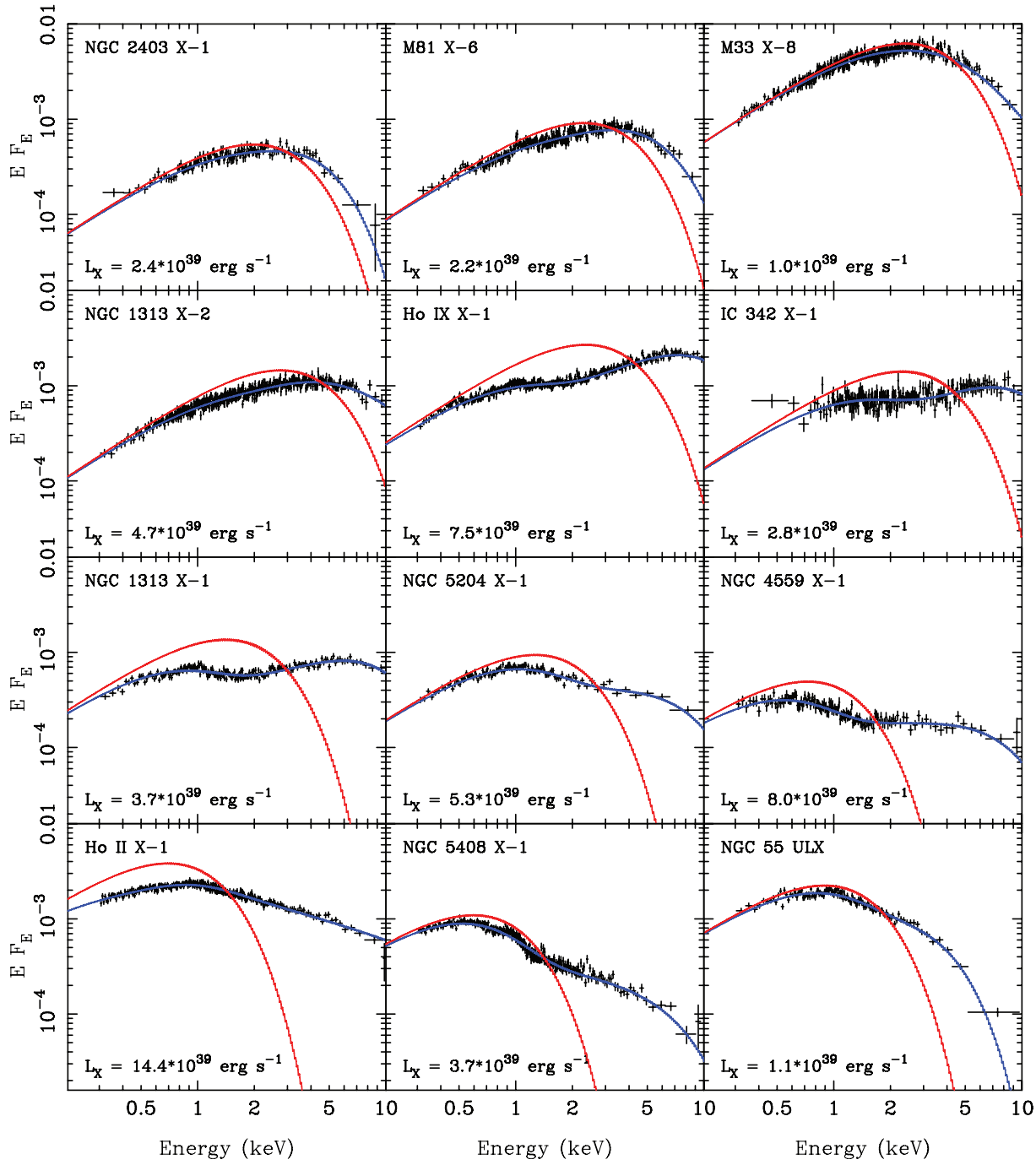

Figure 8. *XMM–Newton* EPIC pn data (black) for all sources in our sample, absorption-corrected and deconvolved with DKBFTH (shown in blue). The 'true' disc spectrum is overplotted in red, this is the disc spectrum that would be observed in each case if the corona was removed. It is evident from these spectral plots that we are observing a variety of spectral shapes. The first four objects (NGC 2403 X-1, M81 X-6, M33 X-8 and NGC 1313 X-2) appear very disc-like in structure and could be representative of the high or very high state. As we move further down the plots, an inflection begins to emerge at ∼2 keV, signifying a break from the standard sub-Eddington accretion states, which we suggest represents a transition to a new super-Eddington accretion state. As the apparent disc temperature cools, the spectrum tips, indicating the possible presence of strong winds enveloping the inner regions of the accretion disc, leading to the most extreme cases (Ho II X-1, NGC 5408 X-1 and NGC 55 ULX).

apply a simplified model often used for such spectra, where the temperature profile in the disc is assumed to be $T \propto r^{-p}$, with p being a free parameter rather than fixed at 0.75 as for standard discs (Watarai et al. 2001). Our data give $0.4 \leq p \leq 0.6$, similar to the $p = 0.5$ expected for advection-dominated discs, but the derived inner-disc temperatures are unrealistically high ($T_{\rm in} \geq 6$ keV) for one-third of our sample. Fig. 4 illustrates this for NGC 1313 X-1, where $T \sim 8$ keV. Plainly, the disc temperature is set by the presence of the high-energy break, but such high inner-disc temperatures are not expected even for stellar mass black holes (Ebisawa et al.

Table 10. The ultraluminous model: DKBBFTH.

Source	TBABS*TBABS*(DKBBFTH)							χ^2/d.o.f.
	$N_{\rm H}{}^a$	$kT_{\rm disc}{}^b$	$R_{\rm c}/R_{\rm in}{}^c$	$R_{\rm in}{}^d$	Γ^e	$kT_{\rm e}{}^f$	τ^g	
NGC 55 ULX	$0.239^{+0.02}_{-0.006}$	$0.38^{+0.02}_{-0.01}$	$1.5^{+0.1}_{-0.2}$	700^{+300}_{-100}	$2.0^{+0.3}_{-0.5}$	$0.79^{+0.1}_{-0.08}$	$10.6^{+0.3}_{-0.5}$	989.1/876
M33 X-8	$0.036^{+0.004}_{-0.006}$	1.03 ± 0.04	$2.7^{+1}_{-0.7}$	65^{+10}_{-6}	$3.6^{+0.1}_{-1}$	6^{+30}_{-4}	$1.5^{+0.2}_{-1}$	1201.9/1244
NGC 1313 X-1	$0.211^{+0.004}_{-0.005}$	$0.60^{+0.03}_{-0.04}$	$2.82^{+0.10}_{-0.07}$	460^{+40}_{-30}	$1.66^{+0.03}_{-0.02}$	$2.19^{+0.2}_{-0.09}$	$7.79^{+0.03}_{-0.02}$	1708.5/1608
NGC 1313 X-2	$0.21^{+0.01}_{-0.02}$	$1.18^{+0.05}_{-0.1}$	$4.3^{+1}_{-0.5}$	130^{+80}_{-30}	$2.5^{+0.1}_{-0.2}$	3^{+6}_{-1}	$3.5^{+0.1}_{-0.2}$	1594.8/1592
IC 342 X-1	$0.55^{+0.08}_{-0.03}$	1.0 ± 0.2	$2.8^{+3}_{-0.8}$	160^{+400}_{-80}	$1.6^{+0.2}_{-0.5}$	$2.4^{+7}_{-0.7}$	$7.9^{+0.2}_{-0.5}$	515.7/508
NGC 2403 X-1	$0.234^{+0.009}_{-0.03}$	$0.85^{+0.08}_{-0.1}$	$2.4^{+0.4}_{-0.6}$	170^{+40}_{-30}	$1.9^{+0.2}_{-0.4}$	$1.003^{+10}_{-0.003}$	$9.7^{+0.2}_{-0.4}$	846.9/835
Ho II X-1	$0.079^{+0.008}_{-0.007}$	$0.30^{+0.02}_{-0.01}$	$5.6^{+1.0}_{-0.1}$	3900 ± 100	$2.53^{+0.02}_{-0.01}$	$13.2^{+1}_{-0.6}$	$1.43^{+0.02}_{-0.01}$	1399.4/1360
M81 X-6	0.19 ± 0.02	$0.98^{+0.08}_{-0.05}$	3.3 ± 0.2	140 ± 40	$2.15^{+0.2}_{-0.07}$	$1.39^{+0.07}_{-0.2}$	$6.87^{+0.2}_{-0.07}$	1080.7/982
Ho IX X-1	$0.121^{+0.008}_{-0.005}$	$1.01^{+0.03}_{-0.04}$	$4.0^{+0.2}_{-0.1}$	220^{+50}_{-30}	1.58 ± 0.03	2.5 ± 0.2	$7.92^{+0.03}_{-0.03}$	2286.9/2109
NGC 4559 X-1	$0.138^{+0.008}_{-0.01}$	$0.31^{+0.06}_{-0.04}$	$2.0^{+0.2}_{-0.1}$	3000^{+3000}_{-2000}	$1.95^{+0.09}_{-0.10}$	$1.9^{+0.6}_{-0.3}$	$6.73^{+0.09}_{-0.10}$	513.8/585
NGC 5204 X-1	0.036 ± 0.007	0.54 ± 0.02	$1.8^{+0.2}_{-0.1}$	610^{+100}_{-90}	2.0 ± 0.2	1.9 ± 0.4	$6.5^{+0.2}_{-0.2}$	889.1/865
NGC 5408 X-1	$0.029^{+0.007}_{-0.004}$	$0.255^{+0.006}_{-0.005}$	$1.47^{+0.01}_{-0.05}$	3000^{+200}_{-40}	$2.31^{+0.04}_{-0.03}$	$1.6^{+0.2}_{-0.1}$	$5.80^{+0.04}_{-0.03}$	1246.5/982

Note. Models are abbreviated to XSPECsyntax: DKBBFTH – energetically coupled disc – Comptonized corona model. Specific notes: [a]external absorption column in units of 10^{22} atoms cm^2, [b]un-Comptonized disc temperature (keV), [c]external radius of corona, [d]inner radius of the accretion disc, [e]photon index, [f]temperature of the Comptonizing corona, [g]τ is not a fit parameter of the model, but is derived from Γ and $kT_{\rm e}$.

2003). However, we caution against interpreting these parameters physically as the model fails to account for the inflection that occurs at ∼2 keV. These slim-disc models cannot simultaneously produce *both* the soft excess at low energies *and* the high-energy break seen in the high-quality data used here, though this deficiency may be hidden in lower signal-to-noise ratio data.

In order to explore the nature of these sources in more detail, we consider a combination of a disc plus Comptonization due to its successes in describing the emission of other accretion-powered BHB systems. Two different Comptonization models are applied to the data, COMPTT and EQPAIR, giving two slightly different approximations to thermal Compton upscattering of accretion disc photons (see Fig. 6). Irrespective of which model is used, we find evidence for a cool, optically thick corona, where the high-energy break is set by the electron temperature of this Comptonizing plasma. The parameters of this corona are rather different than anything observed in any of the standard accretion states of BHBs. It has lower temperature and higher optical depth than even the most extreme optically thick corona seen in the very high state (Done & Kubota 2006). Such material must block our view of the inner disc (Kubota & Done 2004), and most likely also changes the energy dissipated in the disc (Done & Kubota 2006).

We attempt to recover the intrinsic disc spectrum by modelling a corona over the inner disc that both Comptonizes the inner regions of the disc and is energetically coupled to it. Both corona and disc are ultimately powered by gravity, so increasing the power dissipated in the corona at a given radius must mean that the disc is less luminous than expected at that radius (Svensson & Zdziarski 1994; Done & Kubota 2006). Again, the parameters indicate a more extreme version of the very high state, but unlike the phenomenological disc plus Comptonization models, these coupled disc–corona models allow us to infer what the source would have looked like without any corona.

The spectral energy distributions derived on the basis of this model can be put into a potential sequence of ULX spectra, as shown in Fig. 8. The first class are those which have spectra which increase monotonically in νf_ν, with maximum power output at the energy given by the high-energy break. All these sources give a 'hot disc' ($kT_{\rm in} > 1$ keV) in the canonical MCD plus power-law fits, with the 'power-law' producing the additional flux at the softest energies. This is probably due to the MCD model providing a poor description of the broader spectra expected from more realistic disc models (Done & Davis 2008; Hui & Krolik 2008). However, these spectra still look fairly similar to the standard disc spectra seen in the disc-dominated state (NGC 2403 X-1, M81 X-6 and M33 X-8). Small amounts of emission from a hot corona can also contribute to the spectrum at the highest energies (see e.g. the spectral decompositions for the most luminous states on XTE J1817-330 in fig. 4 of Gierliński, Done & Page 2009). We note that all of these ULXs have luminosities $\lesssim 3 \times 10^{39}$ erg s^{-1}, so can be close to Eddington for moderately massive (30–50 $M_\odot$) stellar remnant black holes, similar to that found in IC 10 X-1 (see the Introduction). The next source in the sequence, NGC 1313 X-2, has a spectrum where the high-energy emission seems stronger than expected from a disc-dominated state, so this could instead be a type of very high state, again with a moderately massive stellar remnant black hole. Hence, it appears as though the low-luminosity end of the ULX population could potentially overlap with sub-Eddington processes seen in the BHB, albeit for larger black holes. We will explore this in a future paper by characterizing the properties of the Galactic BHBs at high Eddington fractions in the *XMM–Newton* band pass.

The next category is of those where there is clearly a soft inflection as well as a high-energy break, but where the total power still peaks at the high-energy break (Ho IX X-1; IC 342 X-1; NGC 1313 X-1). These are the ones where the simple disc plus (broken) power-law fits give a cool disc together with a high-energy rollover, which we identify with a new *ultraluminous* state. For these data, the coupled disc–corona models give an intrinsic disc temperature that is not given by either of these observed characteristic energies, and where the effect of Comptonization in an optically thick, low temperature corona, is most marked. These spectra do not correspond to any of the known states, but can form from a more extreme (higher optical depth, lower temperature) version of the very high state corona. These are typically brighter than those in the previous class (though there is also substantial overlap in luminosity), so are most likely super-Eddington accretion flows.

There is then a clear observational sequence of spectral shapes through the sources where the ratio of power between Comptonization (the high-energy peak) and the outer disc (low-energy peak) steadily decreases, from NGC 5204 X-1 and 4559 X-1, to the most extreme systems, namely Ho II X-1, NGC 5408 X-1 and NGC 55 ULX. These are the ones where the inferred intrinsic disc temperature from the coupled disc–corona model is $\lesssim$0.4 keV, far lower than expected from stellar remnant accretion.

To understand these, we look first at what happens physically to the flow as it approaches and then exceeds the Eddington limit. It has long been known that the Eddington limit for a disc is somewhat different than that for spherical accretion (Shakura & Sunyaev 1973). A thin disc, which radiates at the Eddington limit at all radii, has an integrated luminosity $L \sim [1 + ln(\dot{m})]L_{\rm Edd}$, where $\dot{m} = \dot{M}/\dot{M}_{\rm Edd}$ is the mass accretion rate scaled to that which gives the Eddington luminosity for spherical accretion. However, this can only be achieved if excess energy over and above that expected from a constant mass inflow rate, radiating with constant efficiency, is somehow lost from the system. There are two ways to do this, either by changing the mass accretion rate as a function of radius through expelling the excess mass via winds (Shakura & Sunyaev 1973; Begelman, King & Pringle 2006) or by changing the radiative efficiency by advecting the photons along with the flow (slim discs, as above). Importantly, both can operate simultaneously (Poutanen et al. 2007), as indeed is shown in the most recent two-dimensional radiation hydrodynamic simulations of super-Eddington accretion flows (Ohsuga 2005, 2006, 2007; Kawashima et al. 2009; Ohsuga et al. 2009; Takeuchi, Mineshige & Ohsuga 2009).

This then gives a possible framework to interpret our results. It is clear that the objects with $\sim$1 keV disc emission are probably just more extreme versions of the brightest high and very high spectral states known from BHBs. The super-Eddington, ultraluminous state sources are then distinguished by their cool, optically thick coronae and apparently cooler discs. One obvious source of higher optical depth in the corona is the increasing importance of winds as the source starts to accrete past the Eddington limit, and this mass loading of the coronal particle acceleration mechanism leads to lower temperatures of the Comptonizing electrons.

These winds will become increasingly important as the flows become increasingly super-Eddington, completely enveloping the inner regions of the disc–corona out to an increasing photospheric radius (as in SS 433; Poutanen et al. 2007). Hence, the observed temperature decreases in line with the Stefan–Boltzmann law (Shakura & Sunyaev 1973; Begelman et al. 2006; Poutanen et al. 2007). The outflow is inherently (at least) two dimensional, so viewing angle will change the apparent system luminosity (Ohsuga 2006, 2007). We suggest that the most extreme objects seen in our current sample, NGC 4559 X-1, Ho II X-1, NGC 5408 X-1 and NGC 55 ULX,[7] are dominated by reprocessing in a wind, and that much of their luminosity output is channelled into kinetic energy.

Thus it seems most likely that we are seeing the ULX transit between the brightest high and very high states, through to a super-Eddington *ultraluminous* state which is similar to the very high state but with lower temperature and higher optical depth in the corona, to a completely new (hyper-accreting) state where the wind dominates the spectrum. In none of these states do we require the presence of IMBHs to explain the X-ray spectrum; all can be explained by stellar mass black holes at high accretion rates, albeit perhaps black holes up to a few times larger than those known in our own Galaxy.

[7] The relatively low luminosity of NGC 55 ULX may be an effect of its disc being close to edge-on to our line of sight, evidence for which comes from the dipping behaviour seen in its X-ray light curve (Stobbart et al. 2004).

6 CONCLUSIONS

The highest quality data have been collated and utilized to both characterize the spectra of ULXs and to constrain their nature. These show that while some ULXs (typically the lowest luminosity ones) have spectra which are probably similar to the high and (especially) the very high state in Galactic BHBs, the majority show more complex curvature which can be modelled by a cool disc component together with a power law which breaks/rolls over above $\sim$3 keV. This combination of spectral features is not commonly present in any of the known (sub-Eddington) Galactic BHB states, and we therefore propose these features as observational criteria for a new *ultraluminous state* and identify it with super-Eddington accretion flows.

More physical models for these spectra show that they are not well fit by (approximate '*p*-free') slim-disc models as these cannot simultaneously produce both the soft excess and high-energy break. Instead, disc plus Comptonization models give a much better description of this complex curvature, indicating that the break above $\sim$3 keV comes from a cool, optically thick corona. This suggests a more extreme version of the coronae seen in the very high state of BHBs, as might be expected for super-Eddington flows. However, such coronae obscure the inner disc and alter its energetics (Done & Kubota 2006), so we model these effects to recover the intrinsic disc temperatures. Many of these are in the range expected for stellar remnant black holes, showing that the apparent cool disc temperature derived from simple disc models does not require an IMBH. However, there are some objects where the recovered disc temperature (corrected for the corona) is cooler than expected for a stellar remnant black hole. We suggest that these are most likely to represent the most extreme super-Eddington accretion flows, where the wind from the accretion disc becomes so powerful that it envelops the inner disc out to a large photospheric radius, producing the cool spectral component.

There are occasional spectra from BHBs at the highest luminosities which are indeed better described by optically thick Comptonization (GRO J1655-40 and GRS 1915+105: Makishima et al. 2000; Middleton et al. 2006; Ueda et al. 2009). Similarly, the highest Eddington fraction AGN, such as RE J1034+396 (Middleton et al. 2009) and RX J0136-35 (Jin et al. 2009), also show such spectra. We suggest that all these sources are in this new super-Eddington *ultraluminous* accretion state. It now appears that ULXs, rather than revealing a new population of IMBHs, are providing us with a template for accretion at super-Eddington rates. This will have wide applications across many areas of astrophysics, ranging from stellar formation to the growth of quasi-stellar objects. Further studies of ULXs that provide a deeper understanding of this new and crucially important accretion regime are therefore imperative.

ACKNOWLEDGMENTS

We thank the anonymous referee for their constructive comments that have helped to improve this paper. JCG gratefully acknowledges funding from the Science and Technology Facilities Council in the form of a PhD studentship. This work is based on the data from the *XMM–Newton*, an ESA Science Mission with instruments and contributions directly funded by ESA member states and the USA (NASA).

REFERENCES

Abramowicz M. A., Czerny B., Lasota J. P., Szuszkiewicz E., 1988, ApJ, 332, 646
Begelman M. C., 2002, ApJ, 568, L97
Begelman M. C., King A. R., Pringle J. E., 2006, MNRAS, 370, 399
Belczynski K., Sadowski A., Rasio F. A., 2004, ApJ, 611, 1068
Belczynski K., Bulik T., Fryer C. L., Ruiter A., Vink J. S., Hurley J. R., 2009, ApJ, submitted (arXiv:0904.2784)
Beloborodov A. M., 1998, MNRAS, 297, 739
Berghea C. T., Weaver K. A., Colbert E. J. M., Roberts T. P., 2008, ApJ, 687, 471
Colbert E. J. M., Mushotzky R. F., 1999, ApJ, 519, 89
Colbert E. J. M., Ptak A. F., 2002, ApJS, 143, 25
Coppi P. S., 1999, in Poutanen J., Svensson R., eds, ASP Conf. Ser. Vol. 161, High Energy Processes in Accreting Black Holes. Astron. Soc. Pac., San Francisco, p. 375
Cunningham C. T., 1975, ApJ, 202, 788
Davis S. W., Blaes O. M., Hubeny I., Turner N. J., 2005, ApJ, 621, 372
Davis S. W.,, Done C., Blaes O. M., 2006, ApJ, 647, 525
Dewangan G. C., Griffiths R. E., Rao A. R., 2006, ApJ, 641, L125
Dickey J. M., Lockman F. J., 1990, ARA&A, 28, 215
Done C., Davis S. W., 2008, ApJ, 683, 389
Done C., Kubota A., 2006, MNRAS, 371, 1216
Done C., Gierliński M., Kubota A., 2007, A&AR, 15, 1
Ebisawa K., Kubota A., Mizuno T., Życki P., 2001, Ap&SS, 276, 11
Ebisawa K., Życki P., Kubota A., Mizuno T., Watarai K. Y., 2003, ApJ, 597, 780
Fabbiano G., Zezas A., Murray S. S., 2001, ApJ, 554, 1035
Feng H., Kaaret P., 2005, ApJ, 633, 1052
Foschini L., Rodriguez J., Fuchs Y., Ho L. C., Dadina M., Di Cocco G., Courvoisier T. J.-L., Malaguti G., 2004, A&A, 416, 529
Fryer C. L., Kalogera V., 2001, ApJ, 554, 548
Gao Y., Wang Q. D., Appleton P. N., Lucas R. A., 2003, ApJ, 596, L171
Gierliński M., Zdziarski A. A., Poutanen J., Coppi P. S., Ebisawa K., Johnson W. N., 1999, MNRAS, 309, 496
Gierliński M., Done C., Page K., 2009, MNRAS, 392, 1106
Goad M. R., Roberts T. P., Reeves J. N., Uttley P., 2006, MNRAS, 365, 191
Grimm H. J., Gilfanov M., Sunyaev R., 2003, MNRAS, 339, 793
Grimm H. J., McDowell J., Zezas A., Kim D. W., Fabbiano G., 2005, ApJS, 161, 271
Heger A., Fryer C. L., Woosley S. E., Langer N., Hartmann D. H., 2003, ApJ, 591, 288
Hui Y., Krolik J. H., 2008, ApJ, 679, 1405
Humphrey P. J., Fabbiano G., Elvis M., Church M. J., Bałucińska-Church M., 2003, MNRAS, 344, 134
Immler S., Wang Q. D., 2001, ApJ, 554, 202
Jin C., Done C., Ward M., Gierliński M., 2009, MNRAS, in press (arXiv:0903.4698)
Kaaret P., Corbel S., Prestwich A. H., Zezas A., 2003, Sci, 299, 365
Karachentsev I. D. et al., 2002, A&A, 385, 21
Kawashima T., Ohsuga K., Mineshige S., Heinzeller D., Takabe H., Matsumoto R., 2009, PASJ, in press (arXiv:0904.4123)
King A. R., 2004, MNRAS, 347, L18
King A. R., Davies M. B., Ward M. J., Fabbiano G., Elvis M., 2001, ApJ, 552, L109
Kubota A., Done C., 2004, MNRAS, 353, 980
Kuntz K. D., Gruendl R. A., Chu Y. H., Chen C.-H. R., Still M., Mukai K., Mushotzky R. F., 2005, ApJ, 620, L31
Lee H., Skillman E. D., Cannon J. M., Jackson D. C., Gehrz R. D., Polomski E. F., Woodward C. E., 2006, ApJ, 647, 970
Li L. X., Zimmerman E. R., Narayan R., McClintock J. E., 2005, ApJS, 157, 335
Lira P., Ward M., Zezas A., Alonso-Herrero A., Ueno S., 2002, MNRAS, 330, 259
Liu J., Di Stefano R., 2008, ApJ, 674, L73
Liu J. F., Bregman J. N., 2005, ApJS, 157, 59
Liu J. F., Bregman J. N., Seitzer P., 2004, ApJ, 602, 249
Liu Q. Z., Mirabel I. F., 2005, A&A, 429, 1125
McClintock J. E., Remillard R. A., 2006, in Lewin W. H. G., van der Klis M., eds, Compact Stellar X-ray Sources. Cambridge Univ. Press, Cambridge, p. 157
Madau P., Rees M. J., 2001, ApJ, 551, L27
Madhusudhan N., Justham S., Nelson L., Paxton B., Pfahl E., Podsiadlowski P., Rappaport S., 2006, ApJ, 640, 918
Makishima K. et al., 2000, ApJ, 535, 632
Middleton M., Done C., Gierliński M., Davis S. W., 2006, MNRAS, 373, 1004
Middleton M., Done C., Ward M., Gierliński M., Schurch N., 2009, MNRAS, 394, 250
Miller M. C., Colbert E. J. M., 2004, Int. J. Mod. Phys. D, 13, 1
Miller J. M., Fabbiano G., Miller M. C., Fabian A. C., 2003, ApJ, 585, L37
Miller J. M., Fabian A. C., Miller M. C., 2004, ApJ, 607, 931
Mitsuda K. et al., 1984, PASJ, 36, 741
Miyawaki R., Sugiho M., Kubota A., Makishima K., Namiki M., Tanaka T., Tsunoda N., 2006, in Wilson A., ed., Proceedings of the X-ray Universe 2005. ESA Publications Division, ESTEC, Noordwijk, p. 433
Miyawaki R., Makishima K., Yamada S., Gandhi P., Mizuno T., Kubota A., Tsuru T. G., Matsumoto H., 2009, PASJ, 61, 263
Narayan R., Yi I., 1995, ApJ, 452, 710
Ohsuga K., 2006, ApJ, 640, 923
Ohsuga K., 2007, ApJ, 659, 205
Ohsuga K., Mori H., Nakamoto T., Mineshige S., 2005, ApJ, 628, 368
Ohsuga K., Mineshige S., Mori M., Kato Y., 2009, PASJ, in press (arXiv:0903.5364)
Portegies-Zwart S. F., McMillan S. L. W., 2002, ApJ, 576, 899
Portegies-Zwart S. F., Dewi J., Maccarone T., 2004, MNRAS, 355, 413
Poutanen J., Lipunova G., Fabrika S., Butkevich A. G., Abolmasov P., 2007, MNRAS, 377, 1187
Prestwich A. H. et al., 2007, ApJ, 669, L21
Radecke H. D., 1997, A&A, 319, 18
Rappaport S. A., Podsiadlowski P., Pfahl E., 2005, MNRAS, 356, 401
Read A. M., Ponman T. J., Strickland D. K., 1997, MNRAS, 286, 626
Remillard R. A., McClintock J. E., 2006, ARA&A, 44, 49
Roberts T. P., 2007, Ap&SS, 311, 203
Roberts T. P., Warwick R. S., 2000, MNRAS, 315, 98
Roberts T. P., Warwick R. S., Ward M. J., Goad M. R., 2004, MNRAS, 349, 1193
Roberts T. P., Warwick R. S., Ward M. J., Goad M. R., Jenkins L. P., 2005, MNRAS, 357, 1363
Roberts T. P., Levan A. J., Goad M. R., 2008, MNRAS, 387, 73
Saha A., Claver J., Hoessel J. G., 2002, AJ, 124, 839
Schlegel E. M., Pannuti T. G., 2003, AJ, 125, 3025
Schlegel E. M., Barrett P., Singh K. P., 1997, AJ, 113, 1296
Shakura N. I., Synyaev R. A., 1973, A&A, 24, 337
Shimura T., Takahara F., 1995, ApJ, 445, 780
Silverman J. M., Filippenko A. V., 2008, ApJ, 678, L17
Soria R., 2007, Ap&SS, 311, 213
Stobbart A. M., Roberts T. P., Warwick R. S., 2004, MNRAS, 351, 1063
Stobbart A. M., Roberts T. P., Wilms J., 2006, MNRAS, 368, 397 (SRW06)
Svensson R., Zdziarski A. A., 1994, ApJ, 436, 599
Swartz D. A., Ghosh K. K., Tennant A. F., Wu K., 2004, ApJs, 154, 519
Takeuchi S., Mineshige S., Ohsuga K., 2009, PASJ, in press (arXiv:0904.4598)
Titarchuk L., 1994, ApJ, 434, 570
Ueda Y., Yamaoka K., Remillard R., 2009, ApJ, 695, 888
Vierdayanti K., Mineshige S., Ebisawa K., Kawaguchi T., 2006, PASJ, 58, 915
Vogler A., Pietsch W., Bertoldi F., 1997, A&A, 318, 768
Watarai K. Y., Fukue J., Takeuchi M., Mineshige S., 2000, PASJ, 52, 133
Watarai K., Mizuno T., Mineshige S., 2001, ApJ, 549, L77
Wilms J., Allen A., McCray R., 2000, ApJ, 542, 914
Winter L. M., Mushotzky R. F., Reynolds C. S., 2006, ApJ, 649, 730

This paper has been typeset from a TEX/LATEX file prepared by the author.